THE EFFECT OF HEAT TREATMENT ON ACTIVITY OF Pt-Au/C ELECTROCATALYST FOR GLYCEROL ELECTROOXIDATION IN ALKALINE

MS. PANISA LERTTHAHAN
ID: 54910438

**A THESIS SUBMITTED AS A PART OF THE REQUIREMENTS
FOR THE DEGREE OF MASTER OF ENGINEERING
IN ENERGY TECHNOLOGY AND MANAGEMENT**

**THE JOINT GRADUATE SCHOOL OF ENERGY AND ENVIRONMENT
AT KING MONGKUT'S UNIVERSITY OF TECHNOLOGY THONBURI**

2ND SEMESTER 2013

The Effect of Heat Treatment on Activity of Pt-Au/C Electrocatalyst for Glycerol Electrooxidation in Alkaline

Miss Panisa Lertthahan
ID: 54910438

A Thesis Submitted as a Part of the Requirements
for the Degree of Master of Engineering
in Energy Technology and Management

The Joint Graduate School of Energy and Environment
at King Mongkut's University of Technology Thonburi

2nd Semester 2013

Thesis Committee

(Assoc. Prof. Dr. Apichai Therdthianwong)	Advisor
(Assoc. Prof. Dr. Anawat Sungpet)	Member
(Assoc. Prof. Dr. Navadol Laosiripojana)	Member
(Dr. Sumittra Charojrochkul)	External Examiner

Thesis Title: The Effect of Heat Treatment on Activity of Pt-Au/C Electrocatalyst for Glycerol Electrooxidation in Alkaline

Student's name, organization and telephone/fax numbers/email

Miss Panisa Lertthahan

The Joint Graduate School of Energy and Environment (JGSEE)

Division of Energy Technology, King Mongkut's University of Technology

Thonburi (KMUTT), 126 Pracha Uthit Rd., Tungkru, Bangkok 10140, Thailand

Mobile: 08-5071-2811

E-mail: panisa.lertt@gmail.com

Supervisor's name, organization and telephone/fax numbers/email

Assoc. Prof. Dr. Apichai Therdthianwong

Department of Chemical Engineering, Faculty of Engineering

King Mongkut's University of Technology Thonburi (KMUTT),

126 Pracha Uthit Rd., Tungkru, Bangkok 10140, Thailand

Tel. (66) 2-470-9222 ext 404

Fax: (66) 2-470-9325

E-mail: Apichai.the@kmutt.ac.th

Topic The Effect of Heat Treatment on Activity of Pt-Au/C Electrocatalyst for Glycerol Electrooxidation in Alkaline.

Name of student Miss Panisa Lertthahan **Student ID** 54910438

Name of Supervisor Assoc. Prof. Dr. Apichai Therdthianwong

ABSTRACT

The Au-based catalysts were prepared by using the polyvinyl alcohol protected method. The physical and electrochemical properties of the as-prepared catalysts were measured. The catalytic activity and stability of the catalysts having different Au:Pt ratios toward glycerol electrooxidation were measured using cyclic voltammetric and chronoamperometric methods. The CV results showed that the 10%PtAu/C provided the highest current density and the lowest onset potential as compared to the others. The stability of 10%PtAu/C was high which was observed from the chronoamperometric results. To promote the alloy formation between Au and Pt, heat treatment of the catalyst was performed with 10%PtAu/C in a temperature range of 300-700 °C at a heating rate of 10 °C/min of under nitrogen atmosphere. The alloying degree of the heat-treated catalyst increased with increasing heat treatment temperature. Consequently, the significant enhancement of the onset potential of glycerol oxidation was achieved for the catalyst treated at 700°C. However, the heat treatment also promoted sintering phenomenon of the metal particles leading to the decrease of the maximum current density. Therefore, the untreated PtAu/C showed higher performance than the heat-treated one.

Keywords: glycerol electrooxidation, thermal treatment, polyvinyl alcohol (PVA) protection, PtAu/C, Direct Alkaline fuel cell

ACKNOWLEDGEMENTS

I would like to thank the following people who kindly helped with the completion of this research study.

First, I would like to acknowledge my advisor Assoc. Prof. Dr. Apichai Therdthianwong for data analysis, and insightful discussion. Your guidance, advice and support throughout this study were invaluable to me. The degree would not have been completed without your counseling. And the author would also like to thank Assoc. Prof. Dr. Supaporn Therdthianwong for sample providing and helpful discussion.

Second, I would like to extend my sincere appreciation to Assoc. Prof. Dr. Anawat Sungpet, Assoc. Prof. Dr. Navadol Laosiripojana, and Dr. Sumittra Charojrochkul for their valuable time and suggestions and for kindly agreeing to serve as the research study committee.

Third, I would also like to thank the Joint Graduate School of Energy and Environment (JGSEE) for providing me the scholarship and research funds for this study.

Finally, I would like to give a special thanks to my parents for their lifetime love and care. I thank my colleague at Fuel Cell and Hydrogen Research and Engineering Center for all the patience, helpful experiment assistance, inspiriting discussion and encouragement.

CONTENTS

CONTENTS (Cont')

LIST OF TABLES

LIST OF FIGURES

LIST OF FIGURES (Cont')

LIST OF FIGURES (Cont')

LIST OF FIGURES (Cont')

LIST OF SYMBOLS

SYSBOLS		UNITS
a	Lattice constant	nm
Greek Symbols		
β	Width at the peak at the half height	rad
δ	Long-term decay rate	$\%.s^{-1}$
θ	Angle position	^{o}
λ	X-ray wavelength	Å
Subscripts		
ads	Adsorption	
cell	Fuel cell	
fcc	Face-centered cubic	
max	Maximum	
Pt	Platinum	
Au	Gold	

CHAPTER 1
INTRODUCTION

1.1 Rationale/Problem Statement

Fuel cell is a device that generates electricity by a chemical reaction. Hydrogen is the most common fuel. However, glycerol is one of the promising alternative fuel in terms of cost-effectiveness, plentiful, safety, high degree of reduction and with no worse environmental effects [1-5]. In contrast, the glycerol oxidation reaction is slow and therefore it requires the development of effective catalysts. Most of all studies have been shown that gold can catalyze glycerol electrooxidation reaction. Au/C exhibits the higher electrooxidation activity than other metals [6-10]. Furthermore, the gold-based catalyst can be further improved by adding the second metal (Ag, Ru, Cu, Pt, Pd and Cd). The improvement of bimetallic catalyst has been concluded into three different effects: (1) the geometric effect, (2) the electronic effect, (3) the bifunctional effect. The AuPt/C catalyst having high alloying degree shows a higher electrocatalytic activity and stability for the alcohol electrooxidation compared to the AuPt/C catalyst having low alloying degree, which can be ascribed to the enhancement of CO tolerance of formic acid electrooxidation.

For bimetallic catalyst, heat treatment process has significant impacts on structural changes, particle size, size distribution and surface morphology [11-12]. In order to increase the alloying degree of bimetallic catalyst, heat treatment process is considered as a necessary step to improve electrocatalytic activity of the synthesized catalyst.

1.2 Literature Review

1.2.1 Electrooxidation of alcohol

Nowadays, the development of proton exchange membrane fuel cells (PEMFCs) has been increased. PEMFCs using hydrogen as the feed stream has a problem of fuel storage. Therefore, the development of technology in PEMFCs was applied to direct alcohol fuel cells (DAFCs), in which alcohol is fed directly as the fuel. For example, methanol is considered to be one of the most fuel studied for DAFCs because it contains no C-C bonds and easy to oxidize in comparison to alcohol molecules with various carbon atoms. Ethanol is another interesting choice as a liquid fuel for fuel cell because it has high

energy density and the possible production from renewable sources. Nevertheless, the challenge that is interesting is the strong C-C bond breaking [13, 14]. The increased performances have been succeeded by the development of new catalyst support materials. The most active metal for ethanol oxidation is Platinum. Pt has high activity and good stability [15], but it is an expensive metal. Pt should be dispersed on a high surface area support such as Vulcan XC-72R carbon. It has been widely used as a support for Pt catalysts, due to its low cost and high surface area [16]. Moreover, Pt is easily poisoned by carbon monoxide (CO) which is one of intermediate species of EOR. The addition of the second metal such as Tin (Sn), Ruthenium (Ru), Molybdenum (Mo) improved the removal of CO from Pt at a low potential [17]. The DMFCs components are highly optimized. Searching for the optimal catalyst material for the DMFC has been a number of studies. It concluded that PtRu is the best material for the anode and Pt for the cathode [1, 18-23].

Alkaline fuel cell (AFC) is a low temperature fuel cell type that has a liquid alkaline electrolyte between the electrodes and utilizes oxygen or air and hydrogen. These cells have several advantages: the highest performance of all low temperature fuel cells and the possibility to use cheaper catalytic materials such as Ni, Ag or metal oxides [20,22-23] along with noble metals. The disadvantage of these systems is that they are intolerant to CO_2 that forms carbonates with the cations (K^+ or Na^+) in the electrolyte. Nevertheless, the high performance and possibility to use cheap electrode materials are interesting, and therefore PEMFCs with anion exchange membranes (AEM) have been developed during the last decade. With alkaline DAFCs, various liquid fuels have been introduced: methanol, ethanol, ethylene glycol, and glycerol [1-5] being the most reported.

The reactivity of electrooxidation of alcohol on Pd and Au is greatly improved [6, 24]. The reactivity of both metals are lower than Pt. However, there are some preliminary reports on attempting to use Au as an alcohol electrooxidation catalyst in alkaline.

Habibi et al. [6] studied the electrocatalytic oxidation of glycerol in alkaline solution by the Au, Pd and Pt nanoparticles modified carbon ceramic electrode (CCE). From the result in Figure 1.1, Pt|CCE provided the lowest onset potential at about 0.57 V vs. SCE, which is approximately 0.12 V and 0.18 V lower than those obtained from the Pd|CCE and the Au|CCE, respectively.

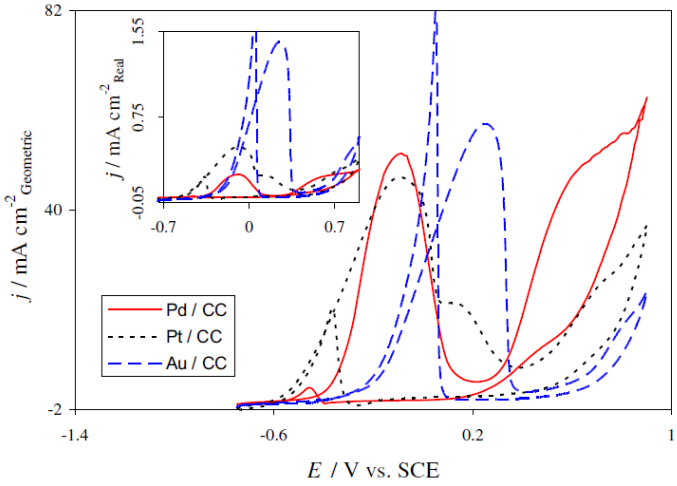

Figure 1.1 CVs of electrocatalysts in 0.3 M NaOH solution + 0.5 M glycerol

The chronoamperometric (CA) results are shown in Figure 1.2. The catalyst activity of the Pt|CCE was higher than that of Au|CCE because Pt can be poisoned by CO easily. Furthermore, the steady state current density of the Au electrode is larger than that of the Pd and Pt electrode indicating that the Au|CCE was the most efficient electrocatalyst compared to other electrodes.

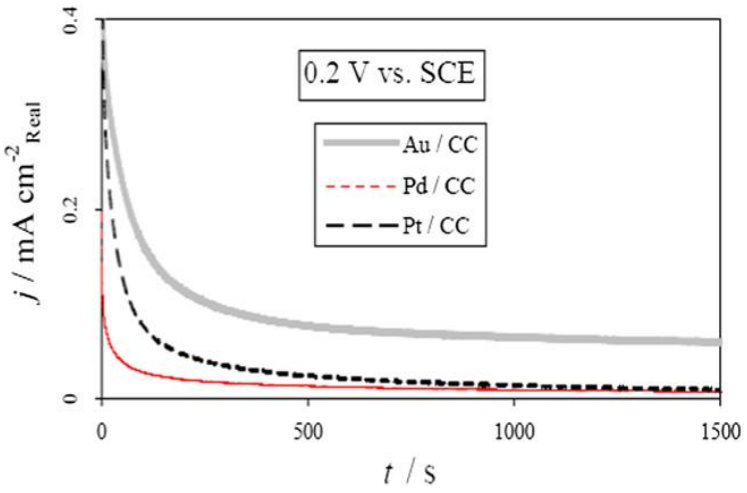

Figure 1.2 Chronoamperograms recorded at different electrode potentials for Pt, Pd and Au modified CCE in 0.5 M glycerol + 0.3 M NaOH solution.

Kwon et al. [25] presented a hypothesis for the electrooxidation of alcohols on gold in alkaline media by assuming that the oxidation of the alcohol to an aldehyde involves two deprotonation steps. The first deprotonation was base-catalyzed, with no essential role

of the metal catalyst. The base-catalyzed reaction followed with pKa which was dependent on the nature of alcohol. Therefore, a lower pKa of alcohol led to higher reactivity. The second deprotonation was fast, provided that the leaving ability of the hydrogen was good, and gold primarily acted as an electron acceptor, although this step likely involved a catalytic interaction with surface bonded hydroxide.

Stuckey [24] studied the glycerol electrooxidation reaction on Pt, Pt-Ru, and Pt-Cr catalysts in both 0.5 M acidic (H_2SO_4) and 0.5 M alkaline (KOH) media. CVs were achieved in both acidic and basic solutions, as shown in Figures 1.3 and 1.4, respectively. It was found that the catalytic activity in terms of lower onset potential and higher current density of all catalysts toward glycerol electrooxidation in alkaline was better performance than that in acid media.

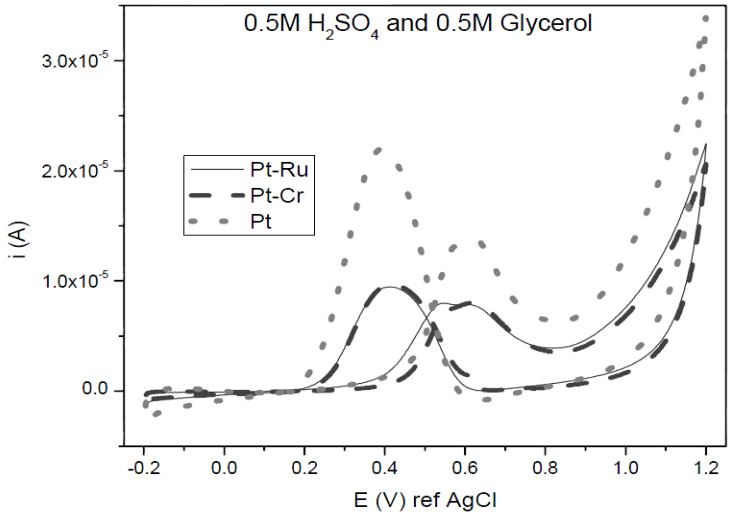

Figure 1.3 CVs of glycerol in acidic media with Pt, Pt-Ru, and Pt-Cr catalysts.

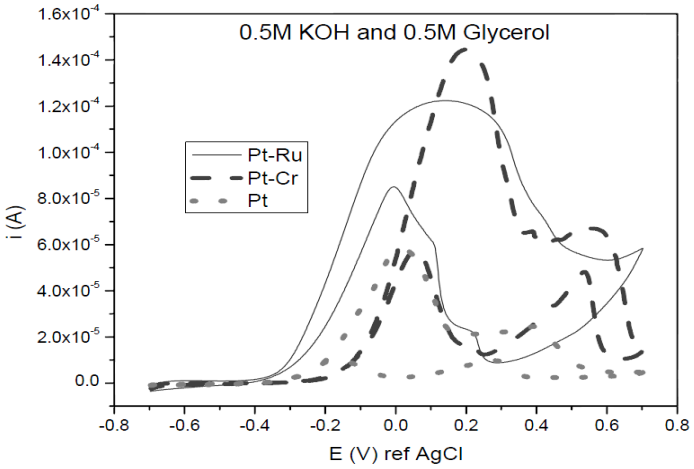

Figure 1.4 CVs of glycerol in alkaline media with Pt, Pt-Ru, and Pt-Cr catalysts.

Zhang et al. [7] compared the activity of different alcohol (methanol, ethanol, n-propanol, isopropanol, EG and glycerol) oxidations on Au electrode, as shown in Figure 1.5. Glycerol is the most active alcohol in electrooxidation reaction on Au. The electrooxidation reaction of glycerol occurred at low potential and provided the highest current density. Then, glycerol oxidations on Au, Pd and Pt electrode are compared in Figure 1.6. The results show that the Au electrode was more active than Pd electrode but less active than the Pt electrode at low potential.

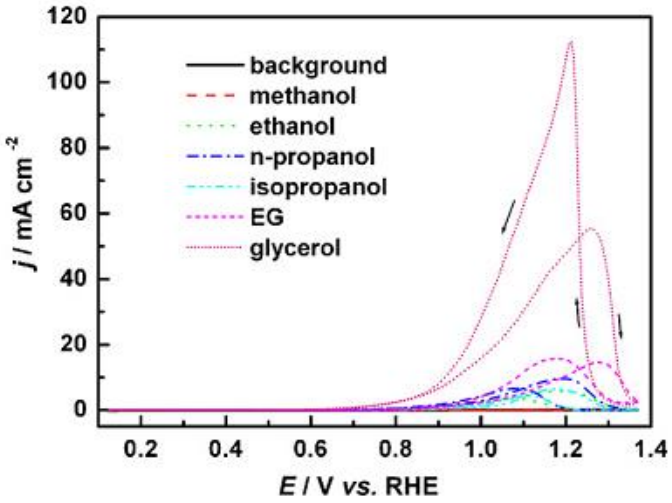

Figure 1.5 CVs of various alcohols (methanol, ethanol, n-propanol, isopropanol, EG and glycerol) electrooxidation on Au electrode in 1.0 M KOH solution containing 1.0 M alcohol.

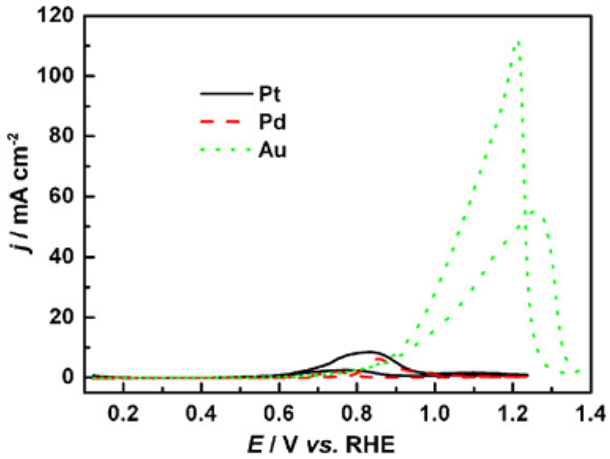

Figure 1.6 CVs of glycerol oxidation on Pt, Pd and Au electrodes in 1.0 M KOH solution containing 1.0 M glycerol.

Yongprapat et al. [8] prepared Au/C and PtRu/C catalysts by using a polyvinyl alcohol protection method for the electrooxidation reaction of ethanol, ethylene glycol and glycerol in alkaline media. Figure 1.7 shows that the cyclic voltammogram of Au/C was similar to that of a bulk Au electrode with a small shift of Au oxide reduction and oxidation potential peaks. Moreover, Figure 1.8 displays the electrooxidation of various alcohols on the Au/C. All alcohols began to oxidize at the same potential which was after the adsorption of hydroxide on Au surface. The current density increased with increasing potential and reached a maximum to around 0.4 V. At this point, the oxide film was formed on Au surface and hindered alcohol electrooxidation. After that, the current density decreased and reached the background current. In the reverse scan, the Au electrooxidation was recovered. The electrooxidation reaction of glycerol and ethylene glycol in the reverse scan were taken place nearly at the same potential as that in the forward scan. Glycerol showed the highest activity, followed by ethylene glycol and ethanol, while methanol was not oxidized. This is because the oxidation reaction of adsorbed alcohol was very fast and the controlled step is adsorption step. The electrooxidation measurement of all the alcohols on PtRu/C at the same condition was shown in Figure 1.9, the most active alcohol on PtRu is methanol, followed by ethanol, ethylene glycol and glycerol. The oxidation of the poisonous species was the rate determining step. The large molecule alcohol occupied more area on Pt surface prevented the access of new coming molecule. In addition, the electrolysis of glycerol yielded formic acid which contributed more than 60% of the total products.

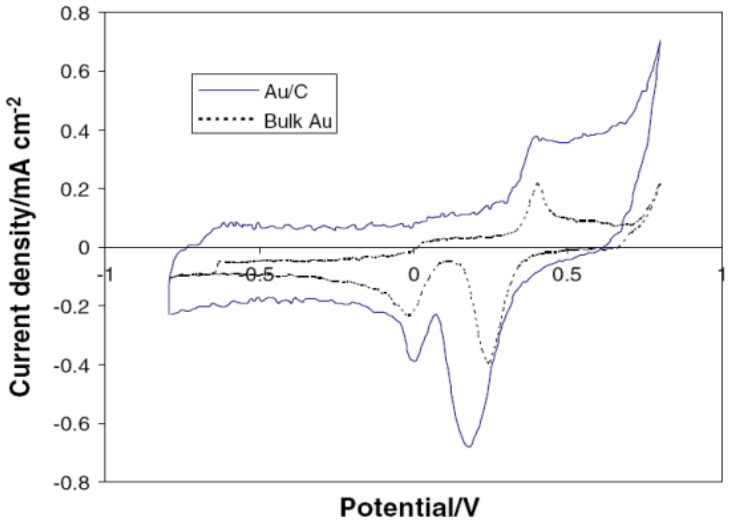

Figure 1.7 CVs of 20 % Au/C and bulk Au in 0.1 M KOH.

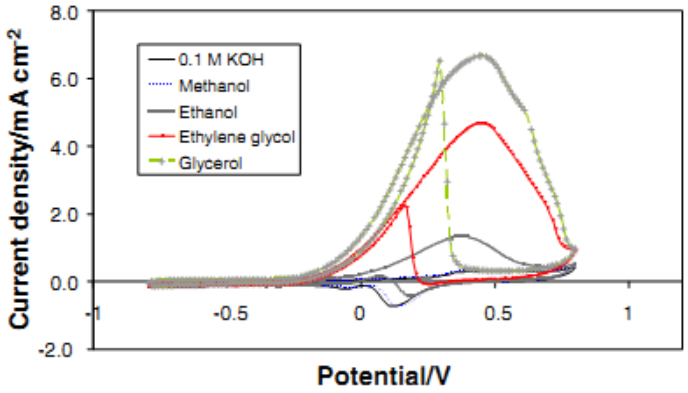

Figure 1.8 CVs of 20 %Au/C in 0.1 M KOH with 0.1 M of its respective alcohols.

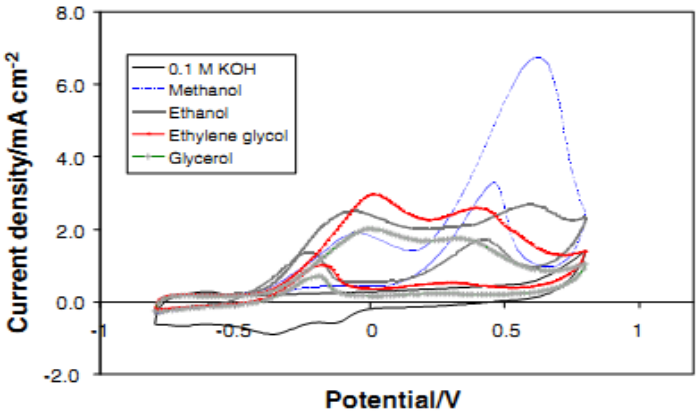

Figure 1.9 CVs of 20 % PtRu/C in 0.1 M KOH with 0.1 M of its respective alcohols.

Yougui et al. [10] studied the employment of non-Pt catalysts for DAFCs. Au and Pd were chosen as all base metals. Upon alloying with Ru, they found that the catalytic activity toward methanol, ethanol and glycerol electrooxidation was greatly improved, as shown in Figures 1.10 and 1.11. For Pd, the catalytic activity towards alcohol oxidation was greatly improved when alloying with Ru. Moreover, the onset potential of all alcohol oxidation was clearly shifted to more negative potential. This indicates the role of bi-functional mechanism achieved by Ru. However, except for ethanol electrooxidation, the performance of PdRu was much lower than that of PtRu. For Au, the catalytic activities were improved upon alloying with Ru. However, the onset potential was not altered. They suggested that the dissociative adsorption of alcohol was the rate determining step on Au, since Ru was unable to accelerate that step, and then alloying Au with Ru did not cause an onset shift. They concludes that Pd and Au exhibited clear activity and the activity could be improved by alloying, however, more works have to be done to improve the activity of these catalysts.

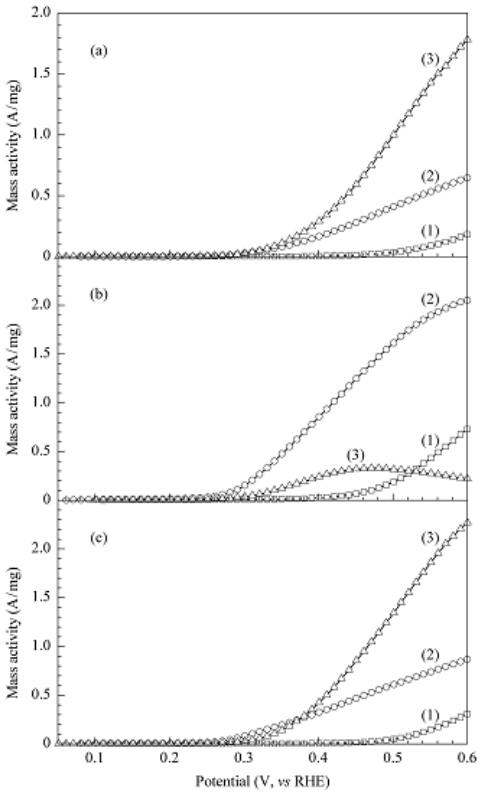

Figure 1.10 Mass specific activity comparisons for (a) methanol, (b) ethanol and (c) ethylene glycol on (1) Pd/C, (2) Pd-Ru(1:1)/C and (3) Pt-Ru(1:1)/C.

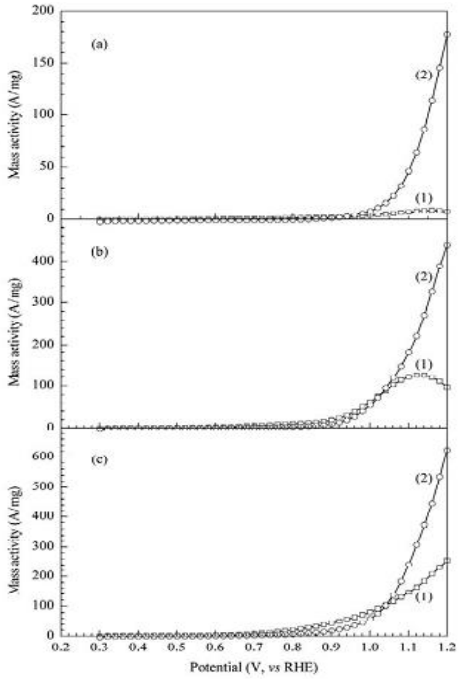

Figure 1.11 Mass specific activity comparisons for (a) methanol, (b) ethanol and (c) ethylene glycol on (1) Au/C, (2) Au-Ru(1:1)/C. [24]

In-Su Park et al. [27] studied the electrooxidation of formic acid on PtAu alloy and Pt-modified Au nanoparticles. The PtAu alloy and Pt-modified Au nanoparticles with different Pt contents were prepared and are designated as as A-1.0, A-4.0, M-0.25 and M-0.75 in Table 1.1. The Pt-modified Au nanoparticles showed higher activities than the pure Pt electrocatalyst in terms of mass-specific current densities as shown in Figure 1.12.

Table 1.1 Descriptions of Au/C, PtAu/C, Pt-Au/C, and Pt/C Electrocatalysts. [27]

Sample	**Description**	**Assumed Pt:Au atomic ratio**	**Metal loading (wt%)**
Au/C	30 wt % Au	-	30
A-1.0	PtAu alloy nanoparticles (PtAu/C)	1.0:1.0	40
A-4.0	PtAu alloy nanoparticles (PtAu/C)	4.0:1.0	40
M-0.25	Pt-modified Au nanoparticles (Pt-Au/C)	0.25:1.0	34.82
M-0.75	Pt-modified Au nanoparticles (Pt-Au/C)	0.75:1.0	42.76
Pt/C	40 wt % Pt	-	40

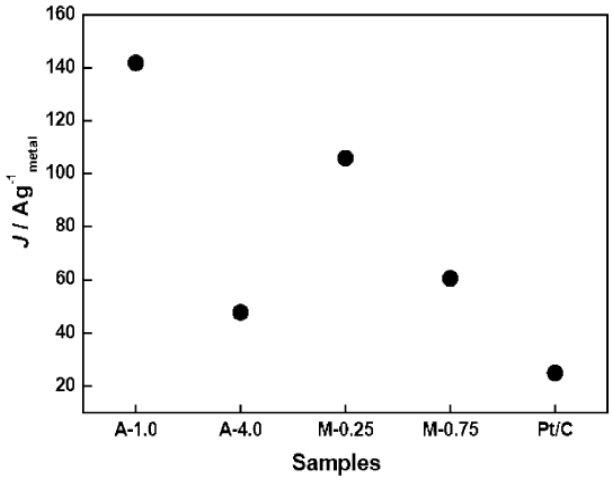

Figure 1.12 Mass-specific current densities: metal-specific current densities (A g^{-1}_{metal}) at 0.3 V vs. NHE. Current densities vs. potential plots were measured in the solution of 0.5 M H_2SO_4 / 1 M HCOOH at room temperature.

The bifunctional effect could not be the mechanism for the enhanced electrocatalytic activity of the PtAu alloy and Pt-modified Au nanoparticles in the formic

acid electro-oxidation, because the Au atoms adsorbed the oxygen species at more positive potentials than did the Pt atoms. Considering the relation between the enhanced activities and the distributions of Pt and Au atoms on the surface of the PtAu alloy and Pt modified Au nanoparticles, the third-body effect might be the possible mechanism for the enhanced activity. However, another possible mechanism could be the electronic modification of Pt which resulted in the strong interaction of HCOOH with Pt. The surface electronic properties of Pt atoms modified by Au atoms could influence the reaction kinetics and the tendency to poison. These results might be due to the enhancement effect of Au atoms and the high Pt utilization in the electrooxidation reaction of formic acid.

The electrocatalytic oxidation of glycerol on PtAu/C catalysts was investigated by Jin et al. [26] using cyclic voltammetry. The PtAu/C catalysts were prepared by chemical reduction with 1:2, 1:1 and 2:1 of Pt:Au composition ratios. The CV results were shown in Figure 1.13 (A) for the PtAu/C, Pt/C and Au/C catalysts in 0.5 M NaOH containing 0.1 M glycerol. The current densities of glycerol oxidation peaks at ca. −0.07 V were about 69.5 mA cm^{-2}, 70.5 mA cm^{-2} and 72.2 mA cm^{-2} for the $Pt_{0.33}Au_{0.67}$/C, $Pt_{0.50}Au_{0.50}$/C and $Pt_{0.67}Au_{0.33}$/C catalysts, respectively. A comparison of the CV curves in Figure 1.13 (A) and (B) revealed that the current density of PtAu/C catalysts was higher than that of Pt/C and Au/C catalysts. This indicated that the PtAu/C catalysts were more active than Pt/C and Au/C for glycerol oxidation. Conversely, the Pt:Au composition ratios had no effect on glycerol oxidation as verified by the CV curves of all PtAu/C catalysts in Figure 1.13 (A).

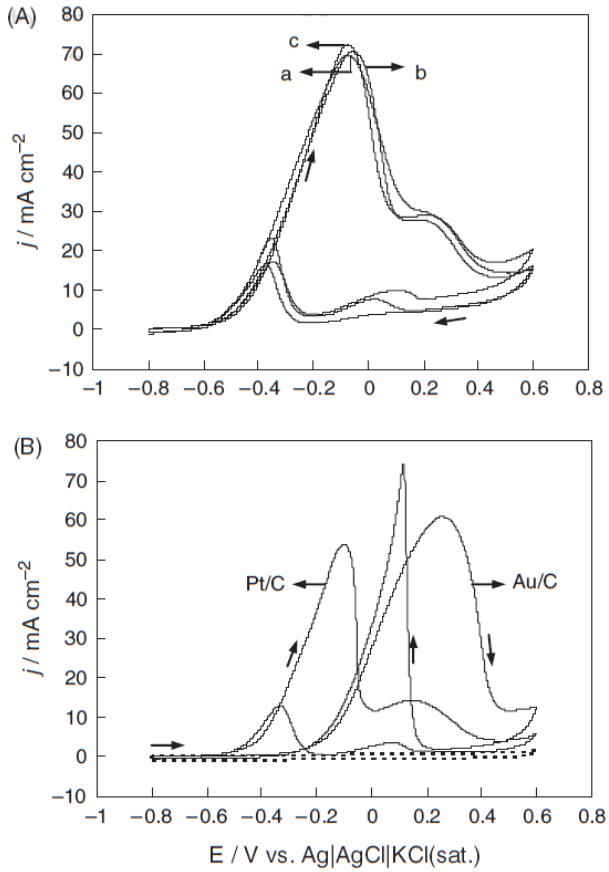

Figure 1.13 CVs of (A) $Pt_{0.33}Au_{0.67}$/C (a), $Pt_{0.50}Au_{0.50}$/C (b) and $Pt_{0.67}Au_{0.33}$/C (c) catalysts, (B) Pt/C and Au/C catalysts, in 0.5 M NaOH containing 0.1 M glycerol. Dotted line in (B) shows CVs of $Pt_{0.50}Au_{0.50}$/C catalyst in 0.5 M NaOH.

Figure 1.14 (A), (B) show cyclic voltammograms of PtAu/C and Pt/C catalysts in 0.5 M H_2SO_4 containing 0.1 M glycerol. The current densities with peak potentials at +0.62 V of $Pt_{0.33}Au_{0.67}$/C, $Pt_{0.50}Au_{0.50}$/C and $Pt_{0.67}Au_{0.33}$/C, are about 6.4, 7.6, and 8.2 mA cm^{-2} for respectively, and about 6.8 mA cm^{-2} for Pt/C catalysts, are observed. The peak current density for a Pt/C catalyst is lower than that for $Pt_{0.67}Au_{0.33}$/C and $Pt_{0.50}Au_{0.50}$/C catalysts but higher than that for $Pt_{0.33}Au_{0.67}$/C catalysts. Namely, the improvement of PtAu/C catalysts over Pt/C catalyst in acidic solution is not as obvious as that in alkaline solution. The differences are still very obvious. For the Au/C catalyst, no oxidation peak is observed in acidic solution.

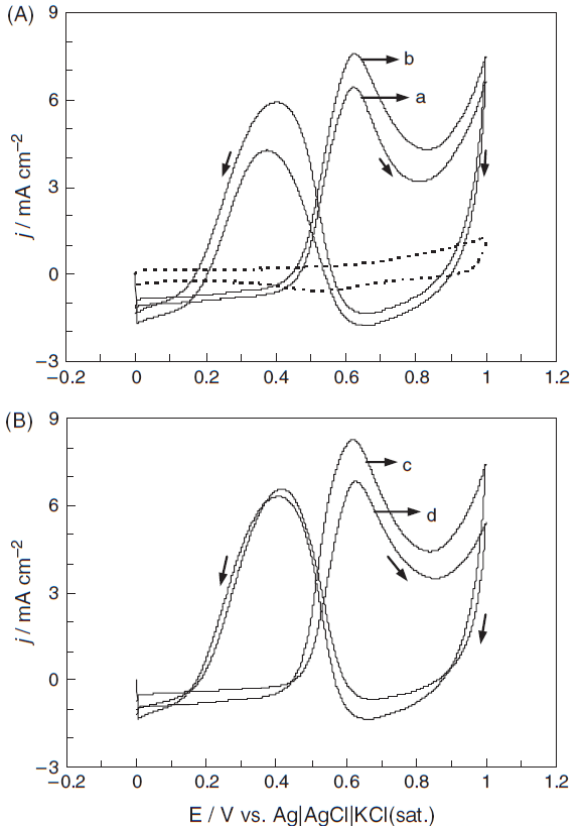

Figure 1.14 CVs of (A) $Pt_{0.33}Au_{0.67}$/C (a), $Pt_{0.50}Au_{0.50}$/C (b) catalysts, (B) $Pt_{0.67}Au_{0.33}$/C (c) and Pt/C (d) catalysts, in 0.5 M H_2SO_4 containing 0.1 M glycerol. Dotted line in (A) shows CVs of $Pt_{0.50}Au_{0.50}$/C catalyst in 0.5 M H_2SO_4.

Several differences for the electrocatalytic oxidation of glycerol on PtAu/C catalysts in alkaline and acidic solutions can be found by comparing Figures 1.13 and 1.14. Firstly, a much more positive oxidation potential and an order of magnitude lower peak current density in acidic solution than in alkaline solution indicated great influence of the pH of media on the reaction. The reaction took place much easier and faster in alkaline solution. In alkaline solution, OH^- involving in the reaction could be both M(Pt, Au)–OH_{ads} and OH^-. In acidic solution, on the other hand, besides at low concentration of OH^-, the adsorption of sulfate anions onto the surface of catalysts has a blocking effect. Secondly, the peak current densities in the negative scan in alkaline solution were larger than that in acidic solution. Finally, Au/C catalyst was active in alkaline solution but inactive in acidic solution. In conclusion, the PtAu/C catalyst exhibited high electrocatalytic activity for the oxidation of glycerol in alkaline solution in terms of onset potential and current density.

1.2.2 Effect of Heat treatment

Yu-Lun Fang [27] investigated the structure property relationships in water-phase for trichloroethene hydrodechlorination (TCE-HDC) reactions on Pd/Au NP catalysts. The carbon-supported Pd/Au NPs with different surface Pd coverage verified their core-shell structure (Au-rich core and Pd-rich shell). As shown in Figure 1.15, the nanostructure transforms from Pd islands to local PdAu alloys. Structure evolution was observed upon heat treatment, in which Pd was in the form of surface Pd ensembles. It can conclude that the metals formed a surface PdAu alloy or a bulk PdAu alloy during heat supply.

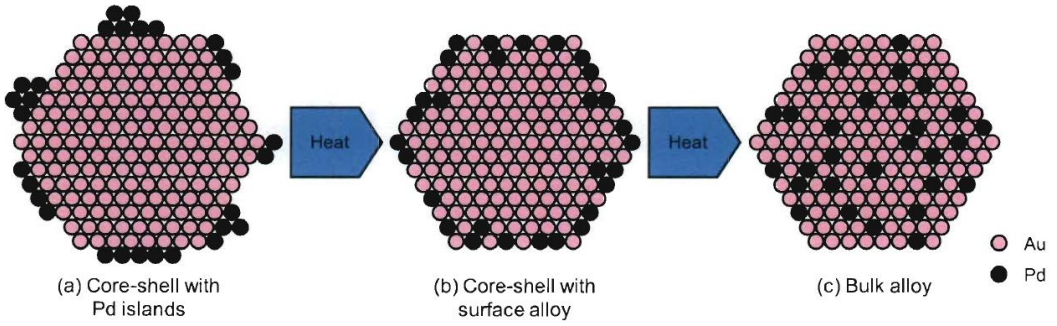

Figure 1.15 Structure transition of Pd/Au NPs with heat treatment, as idealized crosssections for (a) core-shell (Au-rich core, Pd-rich shell) structure with Pd assembled on the shell, (b) core-shell (Au-rich core, Pd-rich shell) structure with surface PdAu alloy, and (c) bulk PdAu alloy.

Min Ku Jeon et al. [28] investigated the effects of heat treatment on PtRu/C catalyst for methanol electro-oxidation. The heat treated PtRu/C catalysts were conducted by reducing the commercial PtRu/C catalyst at 300, 500, and 600^{o}C under H_2 flow. The MOR activity measurement results are shown in Figure 1.16. The current densities with the peak potential at 0.7 V were about 14.8, 30.3, 32.0, and 22.7 mA cm^{-2} for the PtRu-f, PtRu-300, PtRu- 500, and PtRu-600 catalysts, respectively. These results showed that the heat treatment could increase the activity of the PtRu catalyst. The current densities exhibited the highest value in the PtRu-500 catalyst.

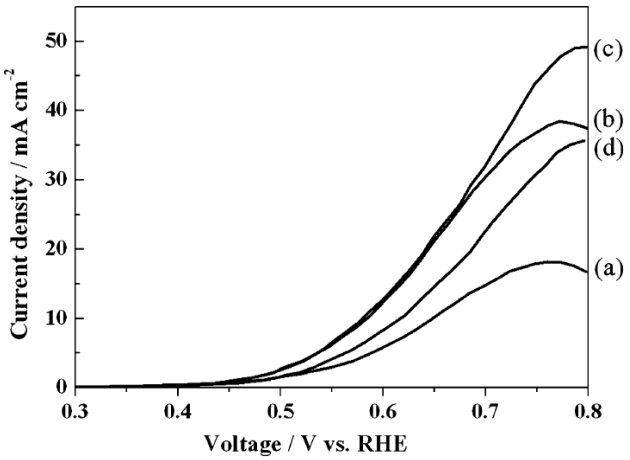

Figure 1.16 Methanol electro-oxidation activities of (a) PtRu-f, (b) PtRu- 300, (c) PtRu-500, and (d) PtRu-600 in 1 M H_2SO_4 solution containing 1 M methanol.

The CV results of the PtRu/C catalysts are shown in Figure 1.17. The shift of the PtO reduction peak, which was near 0.4 V for the PtRu-f catalyst, and moved to higher potentials to reach 0.63 V for the PtRu-600 catalyst. Pure Pt had the reduction peak near 0.72 V, which means that more Pt-like surface was formed by the higher heat treatment temperature. This result suggested that Pt-rich surface formation occurred during the heat treatment.

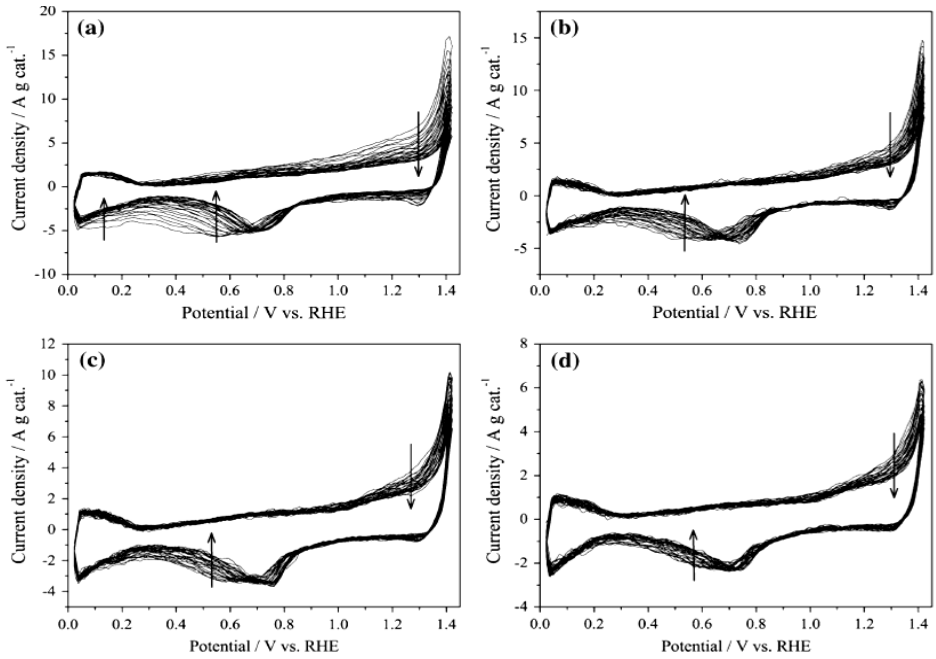

Figure 1.17 CVs of the PtRu-f, b PtRu-300, c PtRu-500, and d PtRu-600 catalysts in 1 M $HClO_4$ solution.

The formation of a Pt-rich surface appeared to be contradictory to the XRD results (Figure 1.18), which shows a higher degree of alloying at higher heat treatment temperatures. However, it can be resolved by realizing that, though a higher degree of alloying was achieved in the bulk by high temperature treatment, the surface property was changed to Pt-rich phase.

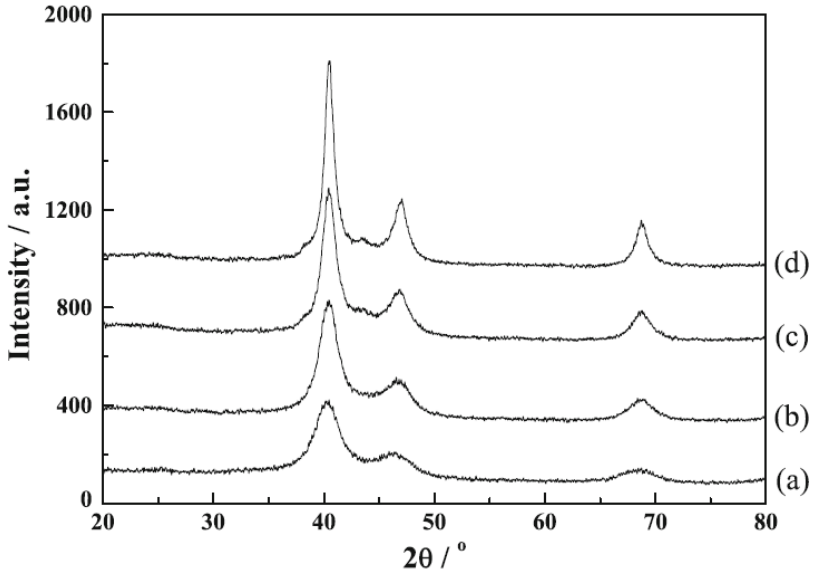

Figure 1.18 XRD patterns of (a) PtRu-f, (b) PtRu-300, (c) PtRu-500, and (d) PtRu-600.

Glycerol, a by-product of biodiesel production from the trans-esterification reaction, has a higher energy density than that of smaller alcohols. The increase of biodiesel demand leads to an increase of glycerol which is the low cost fuel for direct alcohol fuel cells. Direct alcohol alkaline fuel cells (DAAFCs) is a prospect technology for the future. The catalytic reaction in an alkaline is different from in an acid. Au is the metal that is possible to be used in DAAFCs. The catalytic activity of Au for alcohol electrooxidation is superior to that of Pt in alkaline. The catalytic reaction on gold is much faster in the presence of hydroxide ions. The hydroxide adsorption potential on Au surface is far positive. However, adsorption of hydroxide on Pt occurs at a lower potential which enhances the onset potential of alcohol oxidation. However, heat treatment process has a significant impact on structural changes, such as particle size, and surface morphology. In order to increase the degree of alloying of bimetallic catalyst, heat treatment process is considered as a necessary step to improve the electrocatalytic activity of the synthesized catalyst.

The particle size of Au is very important in many reactions. Normally, smaller particles exhibit better catalytic properties. Hence, the deposition of Au on substrate step must be carefully controlled. Au nanoparticle can be prepared by a number of methods such as deposition precipitation, gold sol method, PVA protection methods. The conventional supported Au catalyst contains only small amount of Au, less than 5 %wt. whereas the Au. The loading for fuel cell application was several 10%wt. With this limitation, only few methods are capable in preparation of 5 %wt. – 20 %wt. Au on carbon support with very small particle size.

PVA was proven to be another possible metal sol protector, as described in the work of Chen et al. [29]. They prepared 5% wt. of Au on Vulcan XC-7 carbon. The catalyst was prepared by dropwise adding of $NaBH_4$ into the solution of $HAuCl_4$ with 2% wt. PVA under stirring and then followed by the addition of carbon. After 4 hours of further stirring, the resulting solid was filtered, washed with water and dried in a vacuum oven at 65°C.

The electrocatalytic activity toward glycerol electrooxidation on PtAu/C catalysts in NaOH solution was investigated by Jin et al. [26]. The PtAu/C catalysts were prepared by chemical reduction with 1:2, 1:1 and 2:1 of Pt:Au composition ratios.

In this study, the addition of small Pt content at 5%wt. - 15%wt. to gold-based catalyst was synthesized by PVA protecting method. After that the glycerol electrooxidation reaction of the as-prepared catalyst was performed in KOH solution. Furthermore, the effect of heat treatment temperature on the as-prepared catalyst to the physical and electrochemical characteristic has been investigated.

1.3 Research Objectives

1. To prepare AuPt/C anode catalysts by the PVA protection method and study its performance for glycerol electrooxidation in alkaline media.
2. To study the effect of Au: Pt ratio on glycerol electrooxidation of the catalyst and find a suitable Au: Pt ratio.
3. To study the effect of heat treatment temperature on the activity and stability of the prepared catalysts.

1.4 Scope of Research Work

1. All catalysts studied in this research work were prepared by poly-vinyl alcohol (PVA) protecting method.

2. The metal loading was fixed at 20%. $NaBH_4$ is a reducing agent used to reduce metal ions. $H_2PtCl_6.6H_2O$ and $HAuCl_4.3H_2O$ were used as metal precursors, and carbon black Vulcan XC-72 was utilized as support material.

3. The heat treatment temperatures of 300°C, 500°C, and 700°C, at a heating rate of 10°C/min under 20 ml/min of nitrogen were chosen for heat treatment condition.

4. The physical and electrochemical properties of the catalysts were investigated. The microstructure of the catalyst was examined by X-Ray Diffractometer (XRD). Transmission Electron Microscopy (TEM) images were used to find the particle size and size distribution.

5. The electrocatalytic activity on glycerol electrooxidation was characterized by cyclic voltammogram. The chronoamperometry was employed to measure catalyst stability.

CHAPTER 2
THEORIES

2.1 Fuel cell

A fuel cell is a type of electrochemical cell called a voltaic cell, in which the fuel cell changes chemical potential into electrical potential. The most typical type of fuel cell is the hydrogen fuel cell. Hydrogen fuel cell generates electricity along with water from the reaction of hydrogen and oxygen:

$$H_2(g) + ½O_2(g) \rightarrow H_2O \quad (2.1)$$

This reaction is the same as the combustion reaction of hydrogen. However the electricity is produced instead of heat energy released because the reaction takes place at two separate electrodes.

2.1.1. Basic reactions of fuel cells

Fuel cell reactions are redox reactions. First of all, for the basic fuel cell, the fuel as hydrogen gas (H_2) is fed into flow at anode side, while the oxidant as oxygen gas (O_2) or air is fed at cathode side. Second, H_2 diffuse through to electrode porous that consist of supporting layer, gas diffusion layer, and active layer, while O_2 also diffuse along the opposite side. Third, the reaction of redox is stared. For example, at the anode side on the active (catalyst) layer, hydrogen is oxidized to hydrogen proton (H^+) and electron (e^-) called “oxidation reaction”:

$$H_2(g) \rightarrow 2H^+ + 2e^- \quad (2.2)$$

After that, H^+ is moved through the membrane as solid Nafion® from the anode to the cathode, while e^- is conducted out through carbon support of metal catalyst, carbon at micro-porous layer, carbon backing layer, and bipolar plate as graphite, respectively.

Furthermore, the electron from the anode side will transfer to the cathode side if the fuel cell connects to the electricity load. This electron transfer is called cell current, and also, the difference amount of electron on both side of anode and cathode create the different potential as cell voltage. At cathode side layer of catalyst, O_2 is reduced with H^+ and e- called “reduction reaction”:

$$½O_{2(g)} + 2H^+_{(aq)} + 2e^- \rightarrow H_2O \quad (2.3)$$

From these two reactions, the electrons and protons are produced at the anode and have to pass to the cathode to react with the oxygen. Then to precede the reaction, the electrons must pass through an electrical circuit, while the proton must pass through the electrolyte.

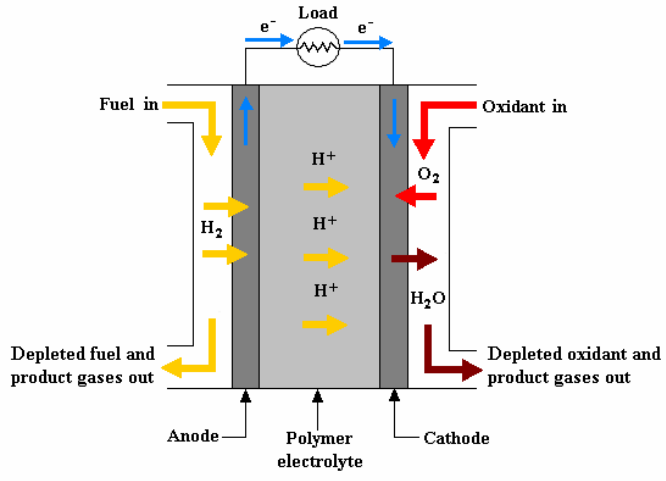

Figure 2.1 Typical components of fuel cells. [31]

2.2 Alkaline Exchange Membrane Fuel Cells (AEMFCs)

This fuel cell is an alkaline type of the polymer electrolyte fuel cells (PEFCs). The components of AEMFC are almost the same as that of PEMFC. The only difference is the type of solid electrolyte. The anion exchange membrane is utilized instead of proton exchange membrane. The conducted species is hydroxide ion, which is moved from the cathode to the anode.

2.2.1 Anode reaction

The reaction at the anode of H_2 fuel cell is hydrogen oxidation reaction (HOR). Since the transported species in AEMFCs is OH^-, H_2 is reacted with OH^- to produce H_2O:

$$H_2 + 2OH^- \rightarrow 2H_2O + 2e^- \quad (2.4)$$

2.2.2 Cathode reaction

At the cathode, the oxygen gas is reduced by electrons and protons from the anode to create hydroxide ions. This reaction is so-called oxygen reduction reaction (ORR). The proposed mechanism is depicted in Figure 2.2.

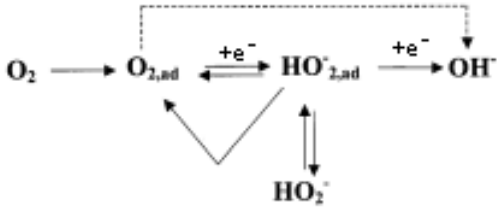

Figure 2.2 The proposed oxygen reduction reaction in alkaline [32].

The reaction can pass through 2 or 4 electrons pathway depending on the dissociation of O-O bond. For 2 electrons pathway, the reaction produces HO_2^- as a final product:

$$O_2 + H_2O + 2e^- \rightarrow OH^- + HO_2^- \quad (2.5)$$

The 4 electrons pathway yields $4OH^-$ as follow:

$$O_2 + 2H_2O + 4e^- \rightarrow 4OH^- \quad (2.6).$$

2.3 Direct Alcohol Fuel Cells (DAFCs)

Direct alcohol fuel cells are fuel cells used alcohol i.e. methanol, ethanol, ethylene glycol, glycerol directly as a fuel. To use liquid fuels, such as low-molecular weight alcohols, have several advantages compared to pure hydrogen, because they can be easy handled, stored and transported. Furthermore, they have relatively high power energy density and can be produced from biomass. However, small molecular weight alcohols have slow anodic kinetic reaction.

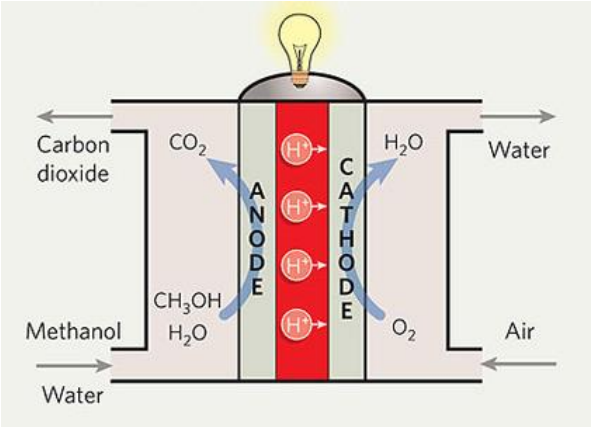

Figure 2.3 Schematic principle of direct methanol fuel cells. [33]

Among the different possible alcohols, methanol is the simplest organic alcohol that has been widely used in DAFCs because it has several advantages: no C-C bond that is

difficult to cleave at low temperatures high solubility is aqueous electrolytes, high power energy density and easy to oxidize. Nevertheless, methanol is toxic, easily flammable and has a low boiling point. Ethanol can be produced by the fermentation of agricultural in the great amount.

Lately, the polyhydric alcohol, the polyol, such as ethylene glycol and glycerol were proposed as new alternative DAFC fuels. Both alcohols are considered renewable. These two alcohols have lower volatility than methanol and ethanol, with acceptable boiling point and freezing point for portable application. Moreover, both are by far lower toxic than methanol.

2.3.1 Direct Alkaline Alcohol Fuel Cells [18]

Recently, the performance of DAFCs has been clearly enhanced by using highly alkaline electrolytes in the direct alkaline alcohol fuel cells (DAAFCs). These fuel cells can use catalysts which are entirely Pt-free or at least with significantly reduced levels of platinum. Nanocatalysts provide huge surface areas for such catalytic reactions.

2.4 Promotion of Effects on Catalytic Properties

Currently, there are more studied bimetallic catalysts because they offer the potential of increased activities and selectivities combined with enhanced stability as compared to their monometallic catalyst. Several groups of bimetallic catalysts have been commercialized for use in industrial environmental treatment and chemical synthesis.

2.4.1 The electronic effect

Upon alloying or using supports, there is a transfer of electron between two or more materials in contact. The flow of electron can be determined from the energy level of electron of each material. According to the thermodynamic equilibrium develops at a contact, the Fermi energy level of electrons of these two surfaces is adjusted to the equal height. To achieve this process, the electron must be transferred from one phase to another one. The property that decides the direction of the electron flow is the work function of the material, which is defined as a minimum energy required for transferring an electron out of the material. The electron will flow from the material with higher work function to the lower one.

The extents of the electrons at the metal-semiconductor can perturb the electronic structure of the metal crystallites and leads to the modifications of their chemisorptive and

catalytic properties. The electronic interaction induced by the electrons transfer [34] can affect the whole metal crystallite is leading the modifications of the electronic structure of metal crystallite, such as:

1. Changes of the d-band population.
2. Shifting of the Fermi level and the work function.
3. Changes in the density of states at the Fermi level.

2.4.2 The bifunctional effect

Under the scope of this mechanism, the reaction is catalyzed by two surface species that show separate functions for each material. One of the most well-known bifunctional catalysts in fuel cell technology is PtRu alloy.

Watanabe and Motoo [35] proposed that the unique properties of the Pt-Ru alloy electrocatalysts are originated from the bifunctional mechanism. Binary or ternary alloys surface consist of two types of metals (A and B) with different adsorbing properties. Type A metal, i.e. Pt, Pd, Ir or Rh is the metals that have an affinity for adsorption and show relatively high catalytic activity towards oxidation reaction of the reactants. Type B, such as Ru, Os, Re, Au or Ag, is the metals that are inert for such a reaction but have an affinity to adsorb the oxygen-containing species. In the oxidation reaction, the rate determining step can be an introduction of oxygen containing species on the B sites or can be a reaction between the adsorbed oxygen species and the intermediate species on the A sites. The rate determining step as described above was then activated by the synergetic action between species on neighboring A and B sites.

The bimetallic mechanism was later supported by the study of Kabbabi et al. [36]. They observed the electrocatalytic oxidation of carbon monoxide and methanol at Pt-Ru bulk alloy electrodes by using Fourier Transform Infrared Spectroscopy (FTIRS) technique. They found that the CO oxidation on Pt-Ru alloy is depended on the concentration of Ru in that the Ru lowers the potential of CO oxidation reaction (0.2 V at 50% Ru) compared to that of pure Pt (0.7 V). The IR spectrum showed that CO is adsorbed on the Pt sites of Pt-Ru alloy, thus the CO oxidation via a bifunctional mechanism is summarized as follows:

$$Pt + CO \rightarrow Pt\text{-}CO_{ads} \quad (2.7)$$

$$Ru + H_2O \rightarrow Ru\text{-}OH_{ads} + H^+ + e^- \quad (2.8)$$

$$Pt\text{-}CO_{ads} + Ru\text{-}OH_{ads} \rightarrow CO_2 + Pt + Ru + H^+ + e^- \quad (2.9)$$

2.5 Heat treatment

Heat-treatment [11] has been known as an important step to improve catalytic activity. Many heat-treatment techniques such as traditional oven/furnace heating, microwave heat-treatment, plasma thermal treatment, and ultrasonic spray pyrolysis have been applied to prepare the electrocatalysts. In general, it involves heating the catalyst in an inert (N_2, Ar or He) or reducing (H_2) atmosphere in the temperature range of 80–900°C for a time period of 1–4 h. Heat treatment of Pt based catalysts has been considered a necessary and crucial step, which has a significant impact on the metal particle size/size-distribution, surface morphology and metal dispersion on the supporting matrix. The benefits of thermal activation or heat-treatment are to remove any undesirable impurity resulting from the preparation stages to allow a uniform dispersion and distribution of the metallic content on the supporting matrix. This can provide improvement in the electrocatalytic activity of the catalysts.

Typically, the role of heat treatment is to promote alloy formation by increasing the mobility of the supported Pt, but the high temperature heat treatment can cause a negative effect on the catalytic activity due to sintering and the growth of Pt particles. However, the mechanisms of the catalysts during the heat-treatment process, the resulting improvement in activity and the relationship between heat treatment and the characteristics of the formed catalysts are so complicated and not fully understood so far [11].

Another typical and well known example is the heat-treatment of macrocyclic metal complexes – though the heat-treatment effect on the properties of such complexes has been well documented, a full understanding of the mechanism of catalytic activity improvement has not yet been achieved. When the catalysts are treated at a desired high temperature in an inert gas atmosphere, the molecular structure is partially or completely destroyed, resulting in a catalyst with much better activity and stability compared with the untreated catalyst. The effect of heat-treatment on catalyst properties is significant in terms of activity improvements as well as in terms of fundamental properties of the catalyst and its support material. These improvements include the loading of the catalyst on the support material, number of catalytically active sites, acid–base properties of the supporting matrix and the distribution of the catalyst particles on the support material.

2.6 Characterization Techniques

This study concerns the preparation of catalysts and the role of the heat treatment process on catalytic activity. The physical and electrochemical properties of catalyst must be intensively investigated. For the physical properties, size and distribution of the precious metal must be observed by x-ray or electron microscopy method. The physical interaction of Au and Pt is observed by x-ray diffraction. In order to study is the activity test of the synthesized catalyst. The catalytic activities of the catalyst toward alcohol oxidation are observed by voltammetric method.

2.6.1. Electrochemical measurement[37,38]

To study the catalytic activity of the nanocatalysts for electrooxidation reaction, two techniques are used in this study. The first technique is cyclic voltammetry (CV) used to study the activity of electrocatalysts. The second technique is chronoamperometry (CA) used to study the stability of electrocatalysts.

2.6.1.1 **Cyclic Voltammetry** (CV)

Cyclic Voltammetry (CV) is an electrochemical technique employ to investigate electrolysis mechanisms that measure the current that develops in an electrochemical cell. CV was performed by cycling the potential of a working electrode, and measures the resulted current. In the forward scan, the reduced species are oxidized producing the anodic current from oxidation reaction. The product generated during the forward scan is available at the electrode surface for the reverse scan. The oxidized species are then reduced in the reverse scan, producing the cathodic current from the reduction reaction. A typical cyclic voltammogram is displayed in Figure 2.4.

2.6.1.2 Chronoamperometry (CA)

Chronoamperometry is an electrochemical technique in which the potential of the working electrode is stepped and the resulting current from faradic processes occurring at the electrode (caused by the potential step) is monitored as a function of time. Limited information about the identity of the electrolyzed species can be obtained from the ratio of the peak oxidation current versus the peak reduction current. However, as with all pulsed techniques, chronoamperometry generates high charging currents, that decay exponentially with time as any RC circuit. The Faradaic current which is due to electron transfer events and is most often the current component of interest decays as described in the Cottrell equation.

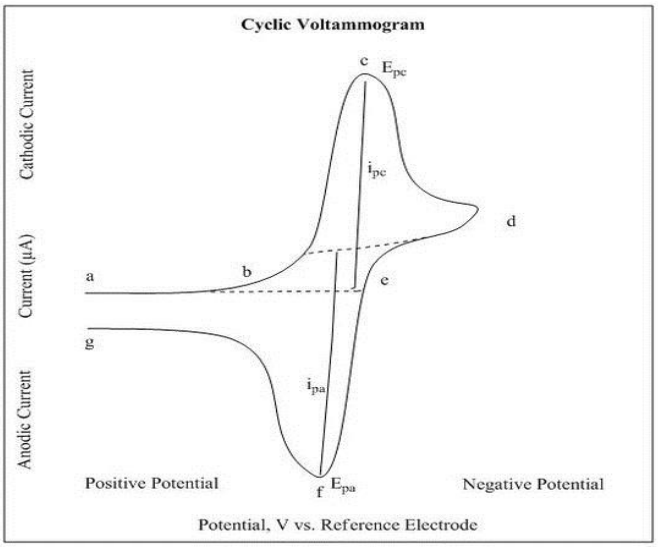

Figure 2.4 Voltammogram of a Single electron oxidation-reduction [37]

In most electrochemical cells this decay is much slower than the charging decay cells with no supporting electrolyte are notable exceptions. Most commonly investigated with a three electrode system. Since the current is integrated over relatively longer time intervals, chronoamperometry gives a better signal to noise ratio in comparison to other amperometric technique.

2.6.2. Transmission Electron Microscope, TEM [39, 40]

The transmission electron microscope is a favorable technique to measure particle sizes and size distribution of a catalyst. TEM operates on the same basic principles as the light microscope but uses electrons as a “light source” and their much lower wavelength make it possible to get a resolution a thousand times better than with a light microscope.

The light source on top of the microscope emits the electrons that go through a vacuum column of the microscope. The TEM uses electromagnetic lenses to focus the electrons into a very thin beam by glass lenses focusing the light in the microscope. The electron beam then goes through the sample. Some of the electrons are scattered and disappear from the beam, depending on the density of the material present. At the bottom of microscope the unscattered electrons hit a fluorescent screen, which gives a rise to a shadow image of the sample with its different parts displayed in varied darkness according to their density.

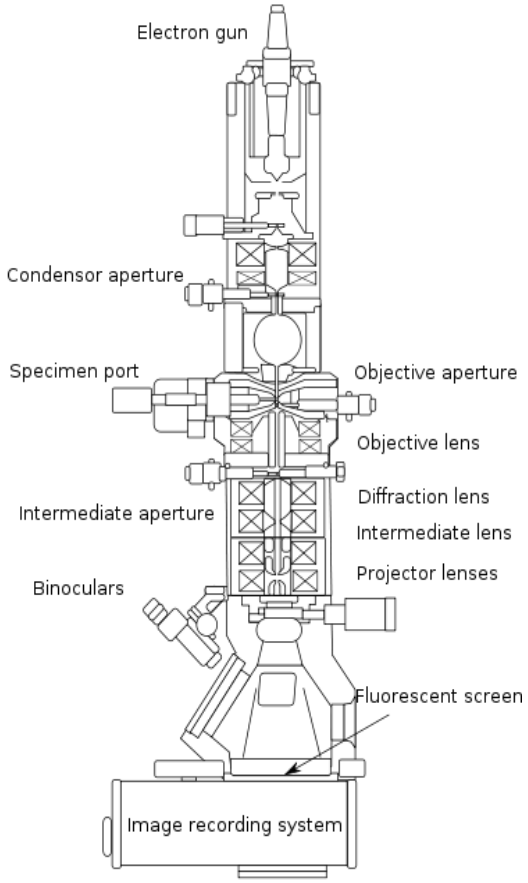

Figure 2.5 Diagram outlining the internal components of a basic TEM system. [40]

2.6.3 X-ray Diffraction, XRD [41, 42]

The XRD is a non-destructive analytical technique used to investigate the structure, composition, lattice parameter, sized broadening, and d-spacing of crystalline material. It can be used to find quantitative information and determine the approximate amount of particle phase in the sample. The principles of XRD are shown in Figure 2.5.

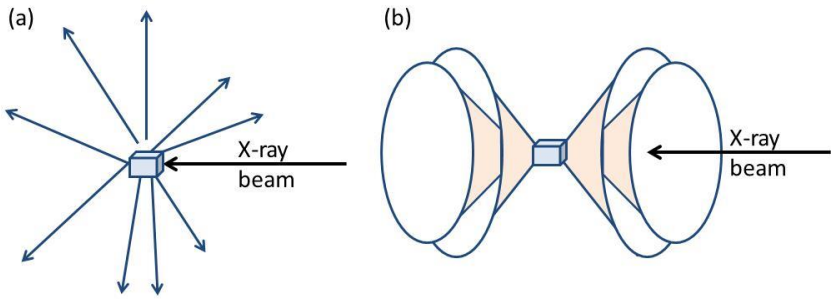

Figure 2.6 Principal of X-ray Diffraction (XRD) [42]

Theoretically, an X-ray beam often produced from a Cu Kα source which has a wavelength of 1.542 Å. It is first filtered to produce a nearly monochromatic beam, and then hits a powder sample. This result leads to emission, absorption, scattering or diffraction. A detector mounted on a goniometer which is rotated around the sample with the same speed at the angle of 0 to 90^{o}C. At the same time, the intensity of radiation is recorded as a function of diffraction angle.

The diffraction of the X-rays beam is shown in Figure 2.6. The average crystal size (d) was estimated by the Debye-Scherrer formula in Eq. (2.10)

$$d = \frac{0.9\lambda}{\beta \cos\theta} \tag{2.10}$$

where d = the average crystal size

λ = the wavelength of the X-rays

β = the width of the peak at the half height

θ = the angle between the incident X-rays and the normal lattice plane

CHAPTER 3
METHODOLOGY

3.1 Methodology

3.1.1 Electrocatalyst synthesis

The Au/C, Pt/C, and PtAu/C with varying weight percentages of Pt at 5, 10, and 15 % were used to study the catalytic activity toward glycerol electrooxidation. All catalysts used in this research were prepared by a PVA protection method. Pt and Au precursors were co-reduced by using $NaBH_4$. The metal loading was fixed at 20%wt of metal. The details of catalyst preparation are as follows:

1. Weigh the calculated amount of Au precursor ($HAuCl_4.3H_2O$) and Pt precursor ($H_2PtCl_6.6H_2O$).
2. Dissolve Au and Pt precursor in DI water.
3. Add 2%wt PVA solution into the solution from Step 2.
4. Add $NaBH_4$ solution dropwise under vigorous stirring.
5. Add Vulcan XC-72 under vigorous stirring and keep stirring for 2 hours.
6. Filter the mixture and wash the filtrate with ethanol and DI water.
7. Dry the filtrate in a vacuum oven.

3.1.2 Heat treatment Method

In order to study the effect of thermal treatment on alloy formation for improving the electrocatalytic performance, the heat treatment technique was applied to the PtAu/C catalyst that exhibited the highest performance on glycerol electrooxidation.

1. A certain amount of 20 wt.% of 10% PtAu/C was inserted into the center of a quartz tube.
2. Then the quartz tube was inserted into the tube furnace.
3. The tube was pre-purged with dry nitrogen gas flowing at 20 ml/min for 30 min to suppress possible surface oxidation of catalyst due to the remaining oxygen within the tube during the heat treatment.
4. The samples were heated at target temperatures of 300, 500, and 700°C for 30 min with heating rate at 10°C/min under nitrogen flow at a rate of 20 ml/min

5. When the heating time was reached, the tube was cooled down under nitrogen gas flowing at a rate of 20 ml/min.

3.1.3 Physical characterization

- X-Ray Diffractometer (XRD)

The characterization of crystallite structure and the crystal size of the as-prepared catalysts were accomplished by an X-Ray Diffractometer (XRD) using Cu Kα as the radiation source. The X-ray diffraction patterns were recorded in the 2θ range of 20°–90° with a step size of 0.4 degree per step and a scan time of 0.4 second per step.

The average crystallite size (d) was estimated by the Debye-Scherrer formula

$$d = \frac{0.9\lambda}{\beta \cos\theta} \tag{3.1}$$

where d = the average crystallite size (nm)

λ = the wavelength of the X-rays (0.15406 nm)

β = the width of the peak at the half height (rad)

θ = the angle between the incident X-rays and the normal lattice plane (°)

The lattice parameter of Au can also be determined from Bragg's Law as follows:

$$a = \frac{\sqrt{2}\lambda_{K\alpha_1}}{\sin\theta_{max}} \tag{3.2}$$

where a = lattice parameter

- Transmission Electron Microscopy (TEM)

TEM is a technique used to examine the particle size and size distribution of metal nanoparticles on carbon support. The average particle size of metal was determined by counting about 400 randomly chosen particles from the relevant TEM images captured at the magnification of 100,000. The average particle size (d_m) was calculated by:

$$d_m = \frac{\sum d_i n_i}{\sum n_i} \tag{3.3}$$

3.1.4 Electrochemical characterization

The voltammetric and chronoamperometric methods are the main methods used to study the catalytic activity of the catalysts toward glycerol electrooxidation. The nature and activity of the electrocatalyst was observed by using cyclic voltammogram. The chronoamperometric method was used for stability test.

3.1.4.1 Electrode Preparation

Before cyclic voltammetry and chronoamperometry tests, the electrodes used in the electrochemical measurements were prepared by dropping the catalyst ink on a glassy carbon electrode (BAS Inc.). The details of the catalyst ink preparation are as follows:

1. Weigh 5 mg of catalyst
2. The micropipette was used to drop the 41.41 μl of 5 wt. % of nafion solution to obtain the nafion 33 wt. % of dry catalyst.
3. Add 1 ml of isopropanol.
4. Ultrasonicate the mixture for 30 min.
5. Drop 11.32 μl of the well-mixed ink onto a glassy carbon electrode with a diameter of 6 mm (or 31.43 μl on an electrode with 10 mm outside diameter) to obtain 200 μg cm^{-2} catalyst.

3.1.4.2 Electrochemical Study

The catalytic activities and stabilities toward glycerol electrooxidation in alkaline solution were studied. The electrochemical experiments were taken by using a three-electrode conventional cell, Au wire and saturated calomel electrodes were used as a counter-electrode and a reference electrode, respectively. The catalyst slurry was loaded on a clean glassy carbon electrode that was used as a working electrode.

Cyclic voltammetry was used to study the catalytic activity of the catalyst. The potential was scanned between -0.8 and 0.7 V at a scan rate of 20 mV s^{-1} in KOH 0.1 mol L^{-1} in presence and absence of 0.1 mol L^{-1} glycerol. The electrolyte was purged by Argon for at least 30 min before used. The activity of the catalysts was determined in terms of current density, potential at maximum current density and on-set potential.

The lead underpotential deposition (upd) method was performed to determine the electrochemical active surface area (ESA) of gold catalyst. The potential was scanned between -0.8 and 0.7 V at a scan rate of 20 mV s^{-1} in KOH 0.1 mol L^{-1} in presence and absence of 1 mmol L^{-1} Pb^{2+} solution. The electrolyte was purged by Argon for at least 30 min before use.

The amperometric curves were recorded in the same electrolyte containing glycerol for 3600 s. The stability of the catalysts was determined from the long-term decaying rate (δ) which was computed based on the steady decaying rate of potentiostatic curves (dI/dt) according to the following equation [8]:

$$\delta = - (100/I_0) \times (dI/dt)_{t>600} \quad (3.4)$$

where δ is the long-term decay rate (% s^{-1}),

$(dI/dt)_{t>600}$ is the average slope of the curve from 600^{th} s to $3{,}600^{th}$ s,

I_0 is the current at the starting point of polarization back extrapolated from the linear current decay curve.

CHAPTER 4
RESULTS AND DISCUSSION

This chapter is divided into 2 main parts, which are the effect of second metal (Pt) Au-based catalyst and the effect of heat treatment temperature on the performance of the as-prepared catalysts. The Au/C and PtAu/C with varied amount of Pt were prepared via the polyvinyl alcohol (PVA) protection method. All the catalysts were characterized by X-Ray Diffraction (XRD) and Transmission Electron Microscope (TEM). Furthermore, the activity and stability of as-prepared catalysts toward the glycerol electrooxidation were examined by using cyclic voltammetric and chronoamperometric methods, respectively. Moreover, the bimetallic catalyst showing the highest performance was selected to examine the effect of heat treatment temperature on the catalyst.

4.1 Effect of second metal on Au-based catalysts.

4.1.1 Physical characterization of as-prepared catalyst

I. XRD characterization

The XRD patterns of all the as-prepared catalysts in the 2θ scan range of 20° - 90° are illustrated in Figure 4.1. In all diffractograms, the wide diffraction peak at around 27º, and 54º belonged to graphite (002) and (004) plane of the hexagonal structure of Vulcan XC-72 carbon (JCPDs Card No. 75-1621). The diffraction peaks at 38º, 44º, 65º, 77.5º, and 82º were designated as the Au (111), Au (200), Au (220), Au (311), and Au (222) planes of Au face-centered cubic (JCPDs Card No. 4-784), respectively. Furthermore, typical diffraction peak of a Pt face-centered cubic including Pt (111), Pt (200), Pt (220), and Pt (311) plane were appeared at 2θabout 40º, 46º, 68º and 81º, respectively.

For all the bimetallic catalysts, XRD diffraction peaks of Au face-centered cubic, there was a shift to higher values of 2θ when compared to Au/C, suggesting the formation of PtAu alloy.

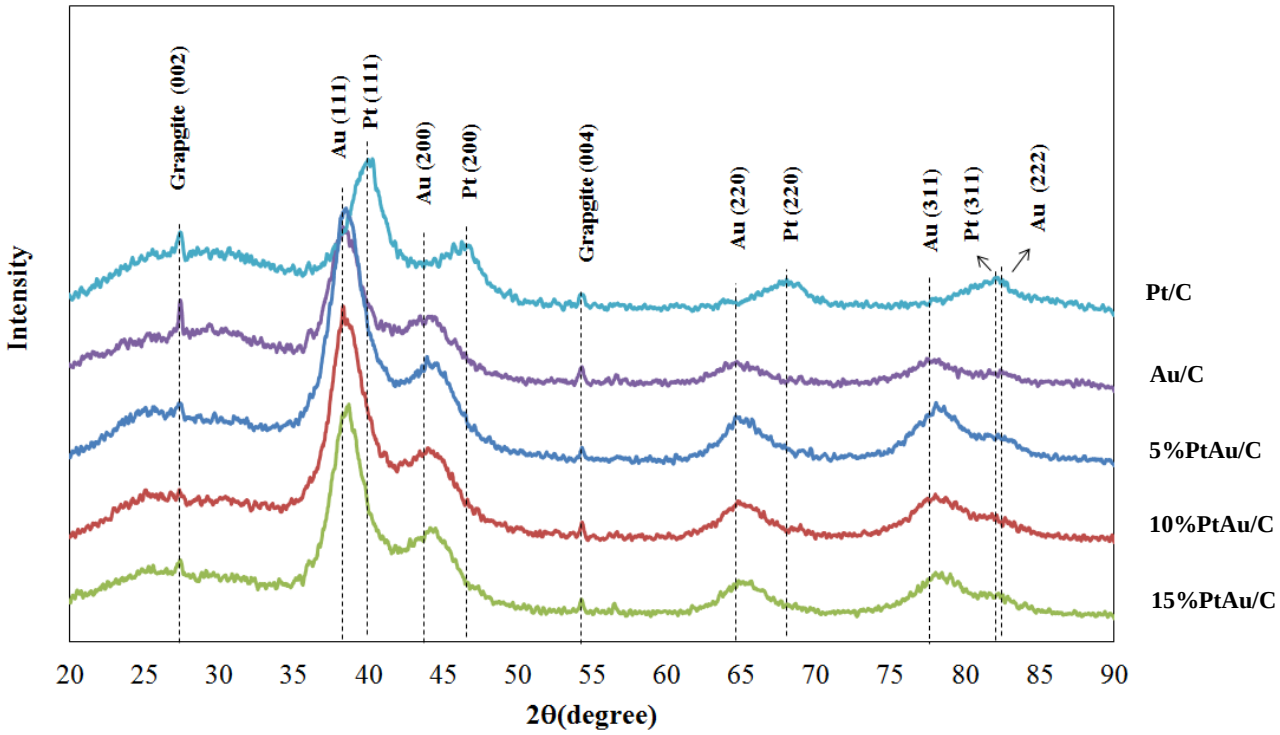

Figure 4.1 X-ray diffractograms of the Pt/C, Au/C, 5%PtAu/C, 10%PtAu/C, and 15%PtAu/C catalysts with step rate at 0.4 sec./step.

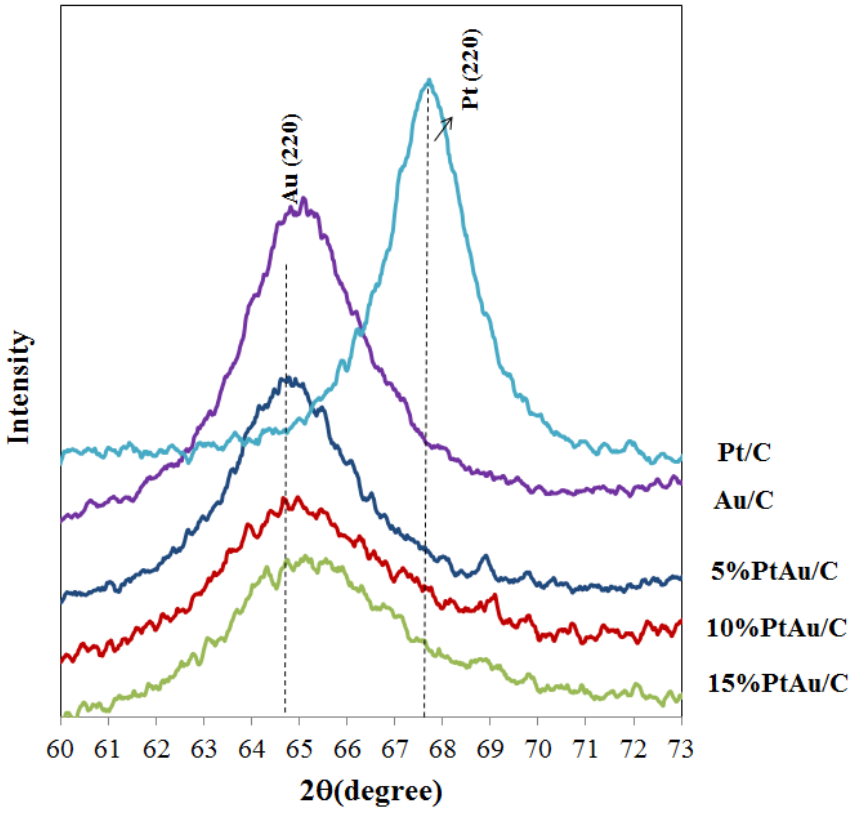

Figure 4.2 X-ray diffractograms of the Pt/C, Au/C, 5%PtAu/C, 10%PtAu/C, and 15%PtAu/C catalysts with step rate at 1.2 sec./step.

The lattice parameters calculated by using the Eq. 4.1 (Bragg's Equation) are shown in Table 4.1.

$$a = \frac{\sqrt{2}\lambda_{CuK\alpha}}{\sin\theta_{max}} \quad (4.1)$$

where

a = lattice parameter of Au in (220) plane

$\lambda_{CuK\alpha}$ = the wavelength of Cu Kα radiation source (0.15406 nm)

θ_{max} = the angular position of the peak maxima (^{o})

Furthermore, the crystallite sizes of all catalysts were determined by Debye-Scherrer's equation as follows :

$$d = \frac{0.9\lambda_{CuK\alpha}}{B_{(2\theta)}\cos\theta_{max}} \quad (4.2)$$

where

d = Crystallite size (nm)

$B_{(2\theta)}$ = Full width at half-maxima peak (rad)

The Au (220) reflection peak was selected for calculating the crystallite size, because it was not affected by another Au plane so that the baseline could be drawn accurately.

From the XRD results of the as-prepared catalysts as listed in Table 4.1, the θ_{max} of all the PtAu/C catalysts were shifted from the Au crystal plane. This indicates the small amount of alloy phase formation between Pt and Au. The shift was the results of the inter-diffusion of Pt and Au atoms in the fcc lattice with elongated Pt-Pt inter-atomic distance [43]. The X-ray diffractrograms of all samples were initially done with high degree step rate at 0.4 second per step. It was found that the adding of Pt in the Au-based catalysts resulted in the decrease of as compared to the Au/C catalyst but the reduction of the lattice parameter was not related to the Pt content. Therefore, the XRD testing was repeated by using a low degree step rate (1.2 second per step) in the 2θ range between 60° and 70° which is the location of the Au(220) peak as displayed in Figure 4.2 and Table 4.1. From the results of using low degree step rate, the lattice parameter, peak position of Au(220)

and crystallite size are in the trend with the Pt content. As the Pt content increased, the Au crystallite size decreased whereas more shifting of the θ_{max} was observed leading to the decrease of the lattice parameter.

Table 4.1 Lattice parameters and crystallite sizes of as-prepared catalysts.

Electrocatalysts	**Lattice Parameter (nm)**		**Peak Position, θ_{max} (degree)**		**crystallite sizes (nm)**	
	0.4 sec./step	**1.2 sec./step**	**0.4 sec./step**	**1.2 sec./step**	**0.4 sec./step**	**1.2 sec./step**
Pt/C	0.3903	0.3914	67.88	67.67	3.0	4.3
Au/C	0.4065	0.4063	64.83	64.87	2.7	3.1
5%PtAu/C	0.4043	0.4049	65.22	65.11	2.7	3.1
10%PtAu/C	0.4048	0.4045	65.14	65.20	2.7	2.5
15%PtAu/C	0.4045	0.4035	65.20	65.37	2.9	2.4

II. TEM characterization

The TEM images of all the synthesized catalysts, where metal particle sizes are identified by black spots, are shown in Figure 4.3. The mean particle sizes of as-prepared catalysts were calculated from more than 400 particles of TEM images as concluded in Table 4.2. The TEM images of Au/C catalyst show well dispersed metal nanoparticles with an average diameter of 3.95 ± 0.6 nm. The Pt nanoparticles were formed an island of metal particles, as illustrated in Figure 4.3 (A). The macromolecule of polyvinyl alcohol might surround many Pt which precipitated and immobilized together on carbon surface was not suitable for the preparation of Pt/C catalyst. Although the Pt/C catalyst formed cluster, each particle still segregated and its particle size was the smallest among all the catalysts prepared by the PVA protection method.

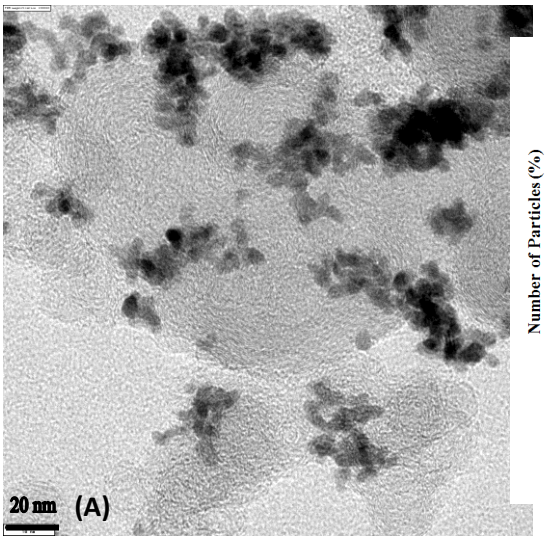
20 nm
(A)

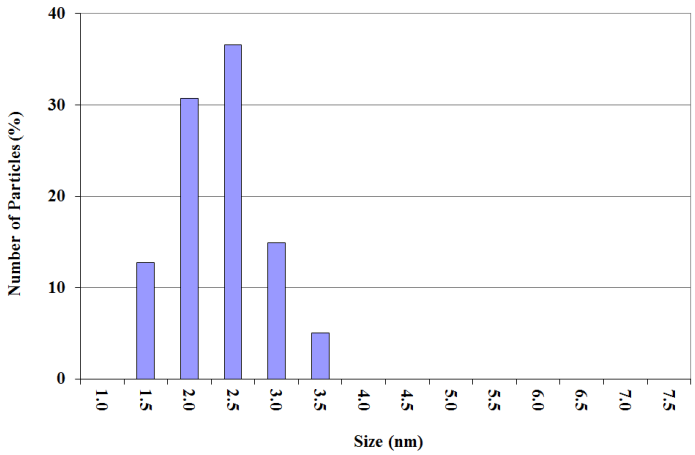
Number of Particles (%)
0
10
20
30
40
1.0
1.5
2.0
2.5
3.0
3.5
4.0
4.5
5.0
5.5
6.0
6.5
7.0
7.5
Size (nm)

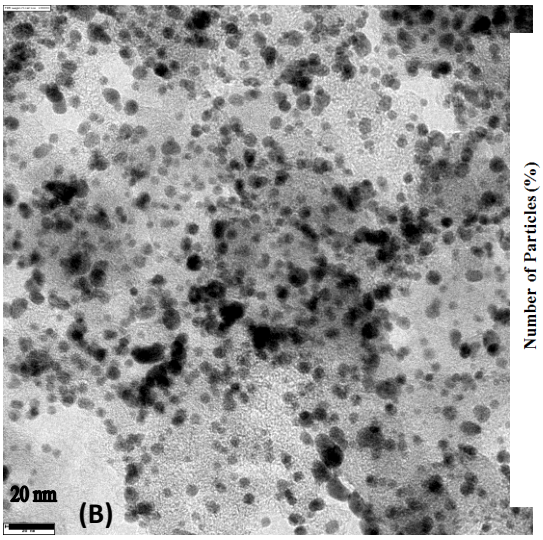
20 nm
(B)

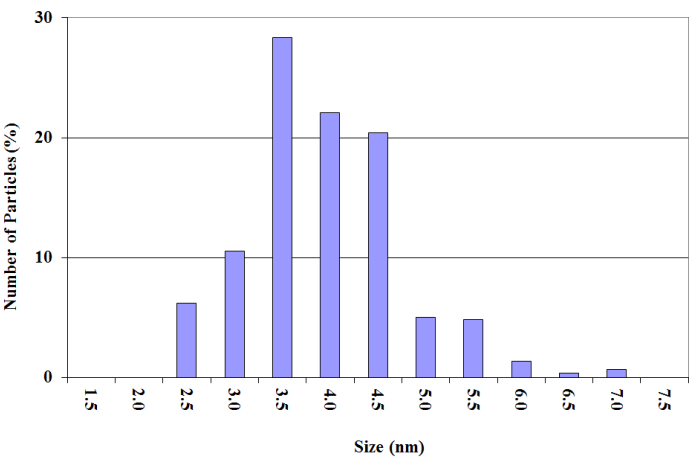
Number of Particles (%)
0
10
20
30
1.5
2.0
2.5
3.0
3.5
4.0
4.5
5.0
5.5
6.0
6.5
7.0
7.5
Size (nm)

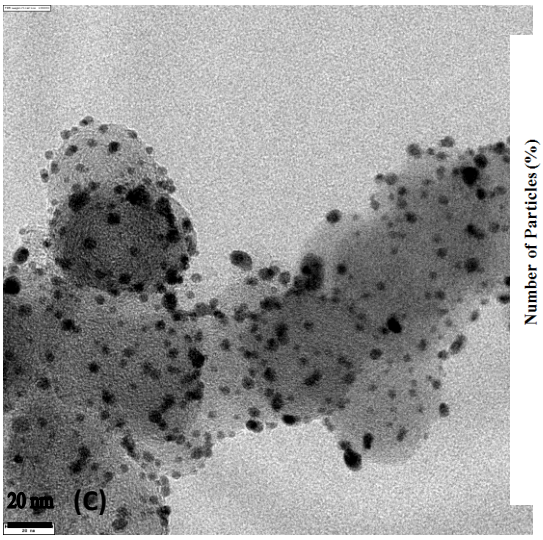
20 nm
(C)

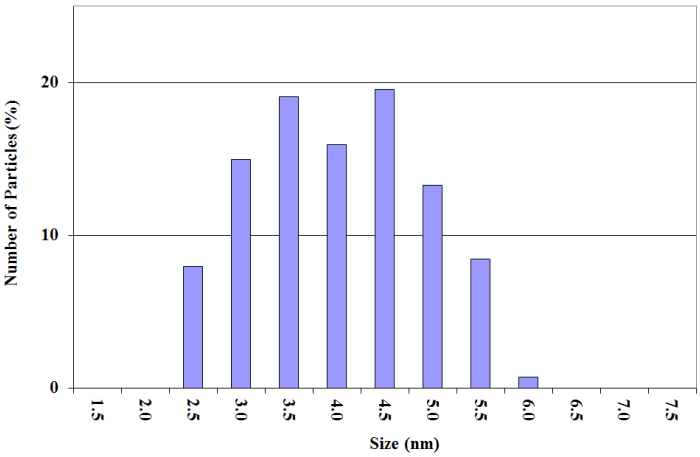
Number of Particles (%)
0
10
20
1.5
2.0
2.5
3.0
3.5
4.0
4.5
5.0
5.5
6.0
6.5
7.0
7.5
Size (nm)

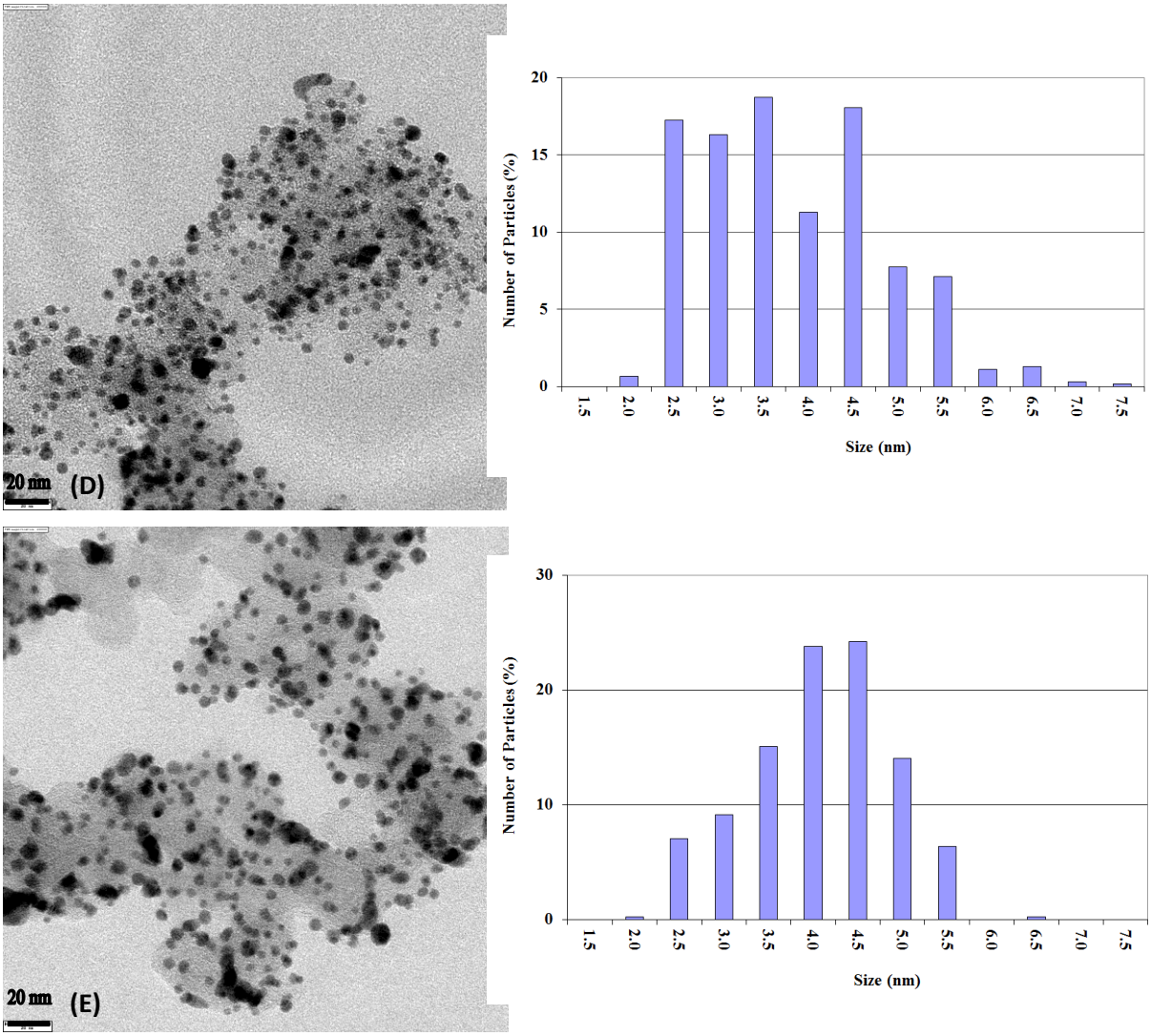

Figure 4.3 TEM images and size distribution of the as-prepared catalysts: (A) Pt/C, (B) Au/C, (C) 5% PtAu/C, (D) 10% PtAu/C, and (E) 15% PtAu/C.

The average particles size of all the bimetallic catalysts (5%PtAu/C, 10%PtAu/C, and 15%PtAu/C) were about the same at around 4 nm. These values were not in the same trend as the crystallite sizes obtained from XRD analysis but their magnitudes were about the same.

Table 4.2 Particle sizes of all of the as-prepared catalysts from TEM

Electrocatalysts	Particle Size (nm)
Au/C	3.94 ± 0.6
Pt/C	2.34 ± 0.4
5% PtAu/C	4.01 ± 0.6
10% PtAu/C	3.81 ± 0.7
15% PtAu/C	4.09 ± 0.5

III. Crystal Structure

The electron diffraction pattern of Au/C was used to characterize the phase of Au nanoparticles, as shown in Figure 4.4. The Au nanoparticle resembles the polycrystalline Au with face center cubic crystal. The reflecting planes of {111},{200}, {220} and {311} were visualized.

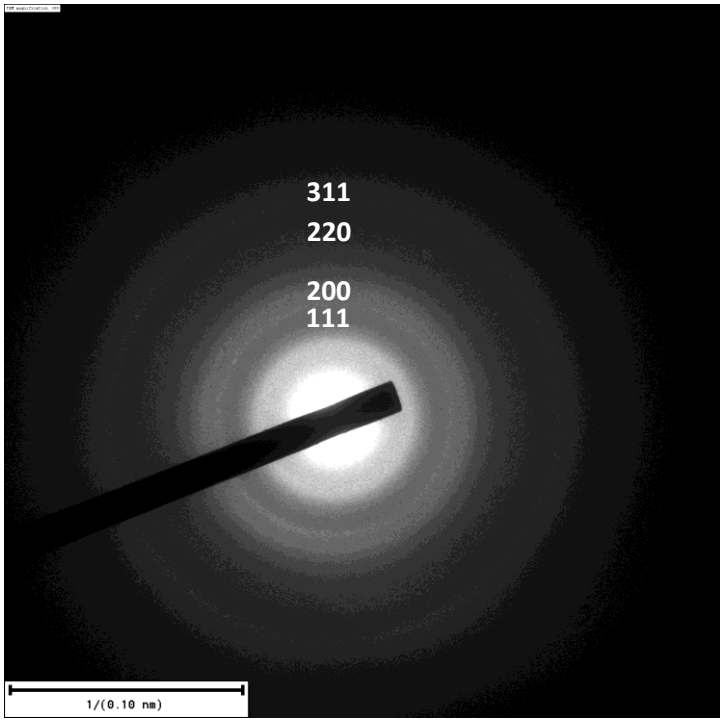

Figure 4.4 Electron diffraction ring patterns of the Au/C catalysts.

4.1.2 Electrochemical characterization of as-prepared catalyst

I. Voltammetric method

Cyclic voltammograms (CVs) of the as-prepared catalysts in 0.1M KOH, as illustrated in Figure 4.5, were performed to observe the characteristics of the catalyst. The potential was repeatly scaned between -0.8 V and +0.7 V vs. SCE at a potential sweep rate of 20 mV s^{-1} until stable CVs were obtained. In the positive scan, the oxidation of the gold surface (gold oxide film formation) was occured at around 0.2 V. The gold oxide film was formed according to the following reactions [44]:

$$Au + OH^- \rightarrow Au\text{-}OH_{ad} + e^- \quad (1)$$

$$Au\text{-}OH_{ad} + 2OH^- \rightarrow Au(OH)_{3,ad} + 2e^- \quad (2)$$

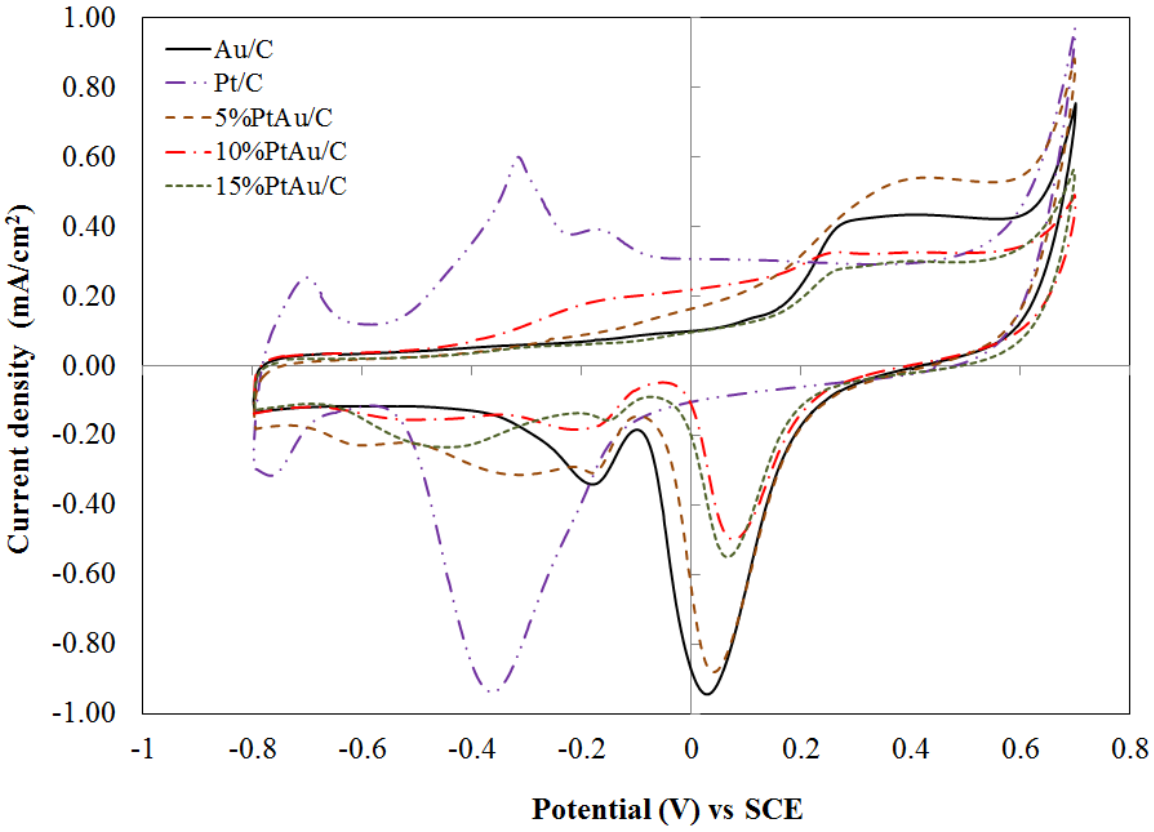

Figure 4.5 Cyclic voltammograms catalysts in 0.1 M KOH solution with a scan rate of 0.02 V s^{-1} at 25ºC for the as-prepared catalysts: Pt/C, Au/C, 5% PtAu/C, 10% PtAu/C, and 15% PtAu/C.

In the negative scan, two reduction peaks of the gold oxide reduction appeared at approximately 0.05 V and -0.2V, which are associated with the reduction of quasi-2D and quasi-3D gold oxide states [8], respectively. The cyclic voltammogram of carbon supported Pt catalysts exhibited two oxidation peaks during the forward scan. The first peak (-0.8 V to -0.6 V) relates to the hydrogen adsorption of the Pt surface. The second peak (-0.6 V to -0.2 V) is associated with the adsorption of OH^- regarding to the following reaction [45]:

$$Pt + H_3O^+ + e^- \leftrightarrow Pt\text{-}H_{ad} + H_2O \quad (3)$$

$$Pt + H^+ + e^- \rightarrow Pt\text{-}H_{ad} \quad (4)$$

$$Pt + H_2O \rightarrow Pt\text{-}OH_{ad} + H^+ + e^- \quad (5)$$

$$Pt + OH^- \rightarrow Pt\text{-}OH_{ad} + e^- \quad (6)$$

Figure 4.6 shows the cyclic votammograms of the as-prepared catalysts in 0.1 M KOH containing 0.1 M glycerol. The onset potentials of Au/C and Pt/C are at -0.201 V. and -0.511 V. vs SCE., respectively. The addition of Pt to Au led to the negative onset potential to -0.453, -0.481 and -0.461 V. vs SCE on 5%PtAu/C, 10%PtAu/C, and 15%PtAu/C, respectively. This shift was possibly caused by the Pt that is more active at lower potential resulting in the lower onset potential as it was also in the work of Fernandes et. al [47].

The activity of the catalyst for glycerol electrooxidation is normally determined by maximum current density of the positive scan peak. From Table 4.3, the maximum current density of Pt/C and Au/C are quite closed to each other, despite occurring at different potential. The maximum current density obtained from 5%PtAu/C and 10%PtAu/C were at 7.97 and 10.79 mA cm^{-2}, respectively, which are higher than that of the Au/C. These results are attributed to the synergistic effect between Au and Pt, i.e., the alteration of the electronic effect provided by the presence of a second metal [46].

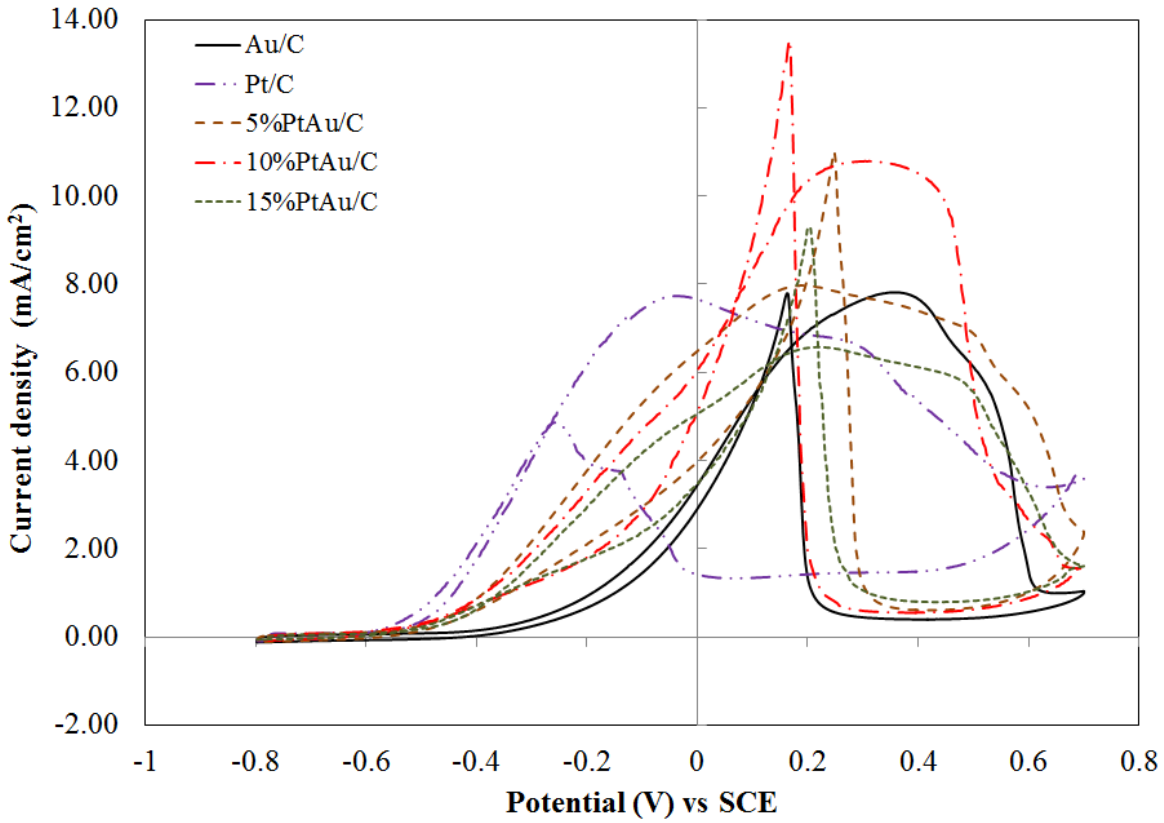

Figure 4.6 Cyclic voltammograms catalysts in 0.1 M KOH solution containing 0.1 M glycerol with a scan rate of 0.02 V s^{-1} at 25ºC for the as-prepared catalysts: Pt/C, Au/C, 5% PtAu/C, 10% PtAu/C, and 15% PtAu/C.

Table 4.3 Maximum current density and onset potential of as-prepared catalysts.

Electrocatalyst	**Maximum current density ($mA.cm^{-2}$)**	**Onset potential (V vs. SCE)**
Au/C	7.81	-0.201
Pt/C	7.73	-0.511
5% PtAu/C	7.97	-0.453
10% PtAu/C	10.79	-0.481
15% PtAu/C	6.57	-0.461

The lead underpotential deposition (upd) method, an accurate method to determine the electrochemical active surface area (ESA) of gold catalyst [50], was applied in this work to determine how the 10% PtAu/C catalyst was more active than the others. The lead upd method was performed by using the cyclic voltammetry in alkaline solution containing Pb^{2+} ion. The lead upd method carried out in a low potential range can be used to identify three low index surfaces of gold facets from the different positions of their stripping peaks in the forward scan [49,50].

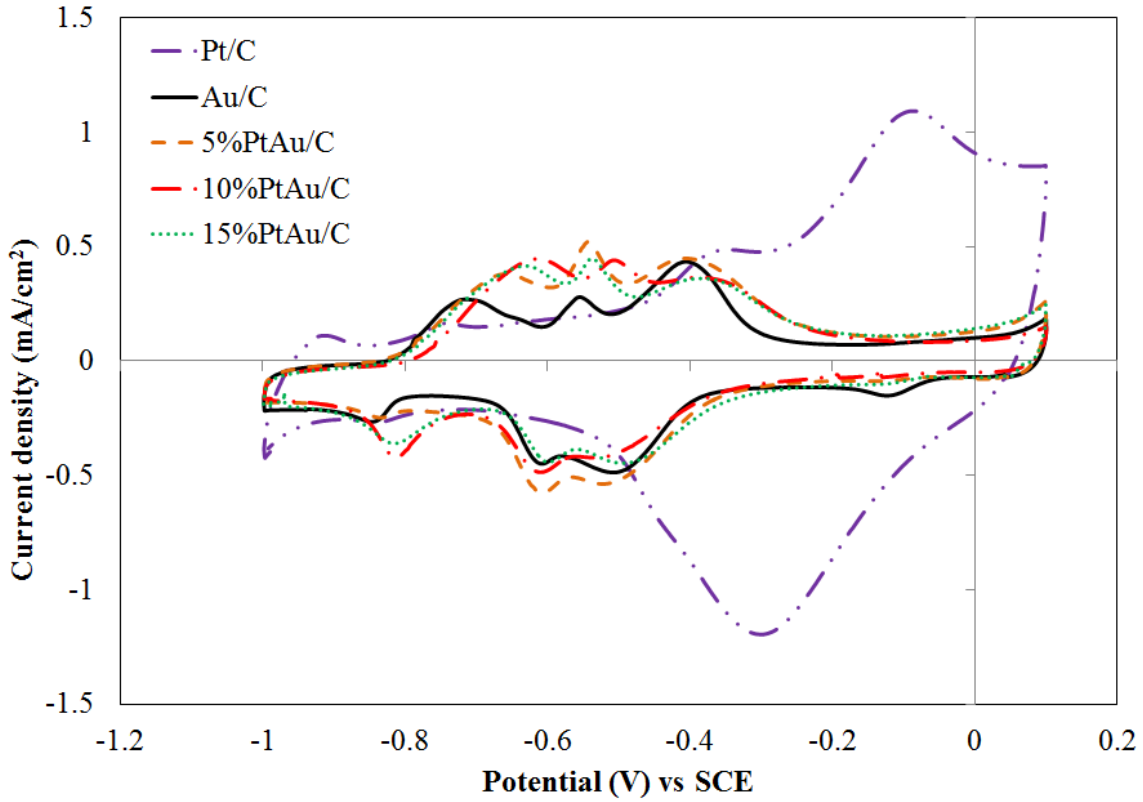

Figure 4.7 Cyclic voltammograms in 0.1 M KOH solution containing 1 mM Pb^{2+} with a scan rate of 0.02 V s^{-1} at 25ºC for the as-prepared catalysts: Pt/C, Au/C, 5% PtAu/C, 10% PtAu/C, and 15% PtAu/C.

Figure 4.7 illustrates the cyclic voltammograms of the catalysts in alkaline solution containing 1 mM Pb^{2+}. In the positive scan, there was no peak appearing in the low potential range for the Pt/C whereas three oxidation peaks were observed for the Au/C and the bimetallic PtAu/C catalysts in the potential between -0.8 V and -0.3 V which was assigned to the Au-(111), Au-(100) and Au-(110) [50]. The ESA of these low index surfaces of gold facets were calculated from the charge density under each peak as

concluded in Table 4.4. From the calculation, 10%PtAu/C catalyst showed the highest ESA value of the Au-(111). This low index surfaces is the most active gold facet since its peak position located at the lowest potential in the positive scan. Therefore, the highest activity of the 10% PtAu/C was mainly attributed to the largest amount of the Au-(111) contained in this catalyst. It was also noticed that the ESA of the Au/C catalyst calculated from the reduction peak of the quasi-2D in Figure 4.5 (38.88 m^2 g^{-1}) was close to that was obtained from the lead upd method.

Table 4.4 The electrochemical active surface area of each low index surface of gold facet, Au-(111), Au-(100) and Au-(110), contained in all the catalysts

Catalyst	**EAS (m^2 g^{-1})**			
	Au-(111)	**Au-(100)**	**Au-(110)**	**Total**
Au/C	13.15	6.00	18.18	37.33
5% PtAu/C	24.65	6.42	30.90	61.96
10% PtAu/C	35.39	3.38	35.02	73.79
15% PtAu/C	32.05	5.16	25.49	62.70

II. Chronoamperometric method

The stability of the catalysts was examined by using the chronoamperometric method. The long-term decay rate was used to determine the stability of the catalysts. Figures 4.8 and 4.9 show the chronoamperometry curve of glycerol electrooxidation 0.1 M glycerol solution containing 0.1 M KOH at -100 and 300 mV vs. SCE. The two potentials were the potential at the maximum current density of the glycerol electrooxidation on Pt and Au surface, respectively.

The current density of all the catalysts drop rapidly at the initial, and then decay slowly during 3600 second or 60 minute. At 300 mV, the long term decay rate obtained from 10% PtAu/C was equal to 2.8 10^{-3}% S^{-1} which was lower than that of other bimetallic PtAu/C catalysts. These results indicated that 10%PtAu/C catalyst had the highest catalytic activity towards glycerol oxidation compared to the others are in agreement with those of the cyclic voltammetry measurements. As a result, it can be concluded that the gold oxide film was formed on higher active Au surface with higher content of Au. Moreover, there are many intermediate species that may poison to catalyst. At -100 mV, all the as-prepared catalyst except Au/C exhibits the higher decay rate than that at 300 mV. Suggesting that

the Pt surface was completely covered by Pt oxide at 300 mV, which might be more active than Au oxide.

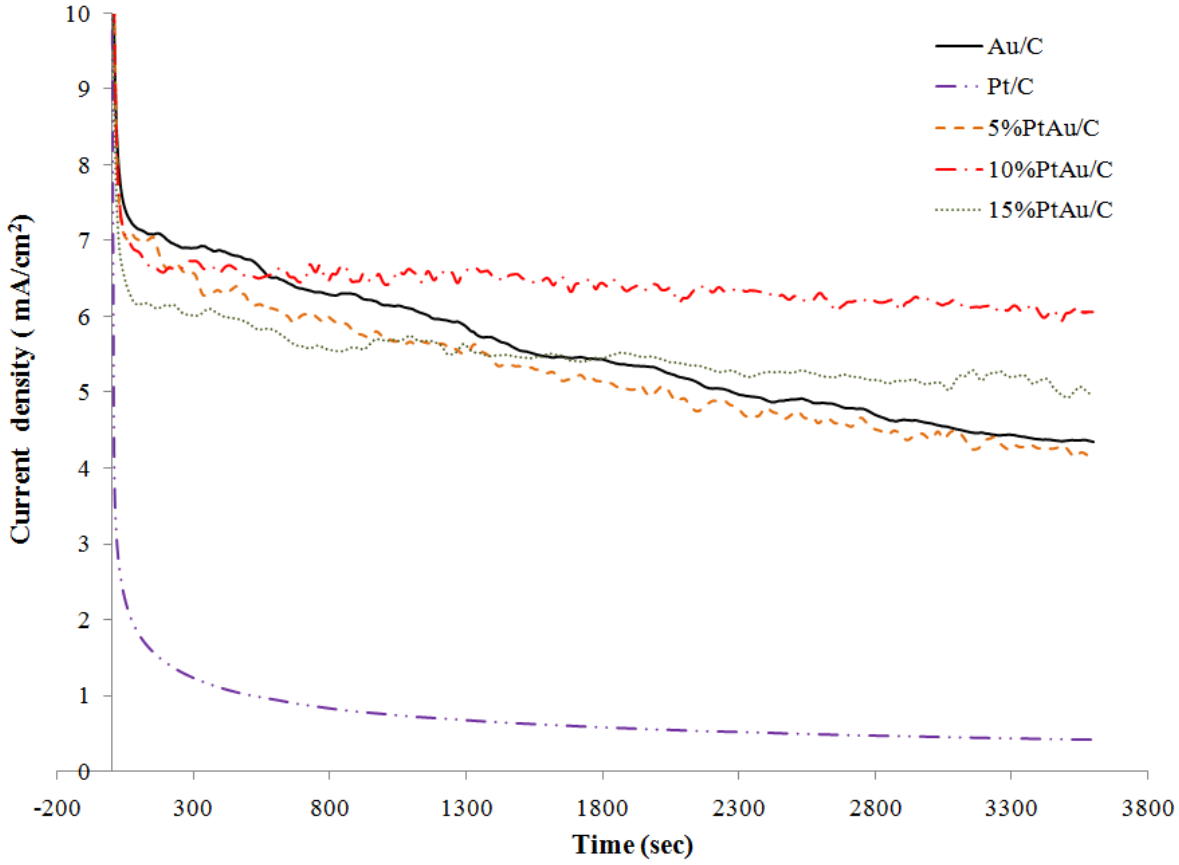

Figure 4.8 Chronoamperometric curves of the as-prepared catalysts at 300 mV vs SCE in 0.1 M KOH solution containing 0.1 M glycerol: Pt/C , Au/C, 5% PtAu/C, 10% PtAu/C, and 15% PtAu/C.

Table 4.5 Final current density and decay rate of the as-prepared catalysts at 300 mV vs. SCE for 60 min

Electrocatalysts	**Final current density ($mA.cm^{-2}$)**	**Decay rate ($10^{-3}\%.s^{-1}$)**
Au/C	4.353	10.901
Pt/C	0.415	16.728
5% PtAu/C	4.159	10.089
10% PtAu/C	6.066	2.827
15% PtAu/C	4.957	3.751

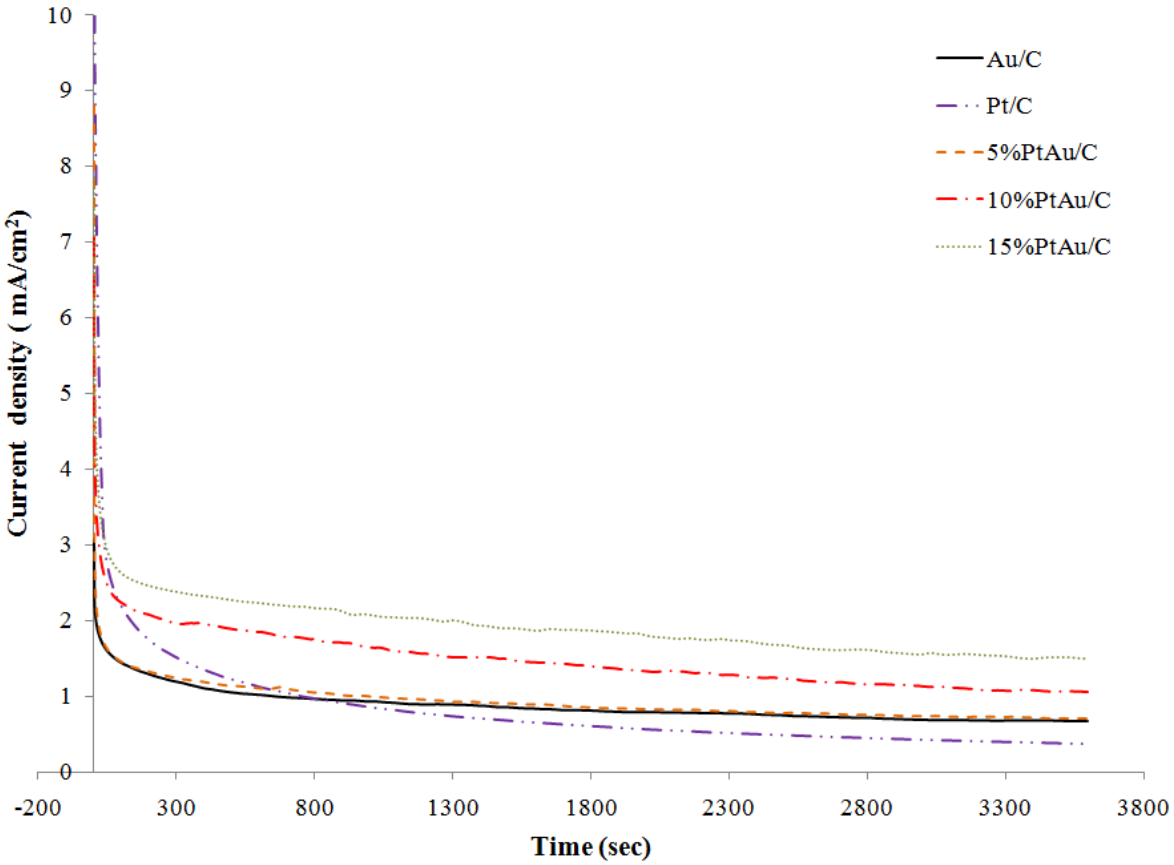

Figure 4.9 Chronoamperometric curves of the as-prepared catalysts at -100 mV vs SCE in 0.1 M KOH solution containing 0.1 M glycerol: Pt/C, Au/C, 5% PtAu/C, 10% PtAu/C, and 15% PtAu/C.

Table 4.6 Final current density and decay rate of the as-prepared catalysts at -100 mV vs. SCE for 60 min

Electrocatalyst	**Final current density ($mA.cm^{-2}$)**	**Decay rate ($10^{-3}\%.s^{-1}$)**
Au/C	0.681	10.671
Pt/C	0.381	20.124
5% PtAu/C	0.707	11.289
10% PtAu/C	1.066	13.316
15% PtAu/C	1.502	10.624

4.2 Effect of heat treatment temperature on the catalysts toward glycerol electrooxidation.

The effect of heat treatment temperature on PtAu/C for glycerol electrooxidation in alkaline was investigated. The 10% PtAu/C was chosen to use in this study because of its high activity as observed in previous section. The untreated PtAu/C and thermal-treated PtAu/C with different heat treatment temperature were prepared and are designated as H-300 10% PtAu/C, H-500 10% PtAu/C, and H-700 10% PtAu/C, as shown in Table 4.7.

Table 4.7 Descriptions of 10% PtAu/C electrocatalysts with thermal-treated and un-treated processes.

Electrocatalyst	Description
10% PtAu/C	Un-treated catalyst
H-300 10% PtAu/C	10% PtAu/C with heat-treated at 300°C
H-500 10% PtAu/C	10% PtAu/C with heat-treated at 500°C
H-700 10% PtAu/C	10% PtAu/C with heat-treated at 700°C

4.2.1 Physical characterization of heat-treated 10%PtAu/C

I. XRD characterization

The XRD patterns of all the heat treated catalysts in the 2θ scan range of 20° - 90° are displayed in Figure 4.10. In the diffractograms, the wide diffraction peaks at around 27º, and 54º assigned to graphite (002) and (004) plane of the Vulcan XC-72R carbon were observed. The diffraction peaks at 38º, 44º, 65º, 77.5º, and 82º are corresponding to Au (111), Au (200), Au (220), Au (311), and Au (222) planes of Au face-centered cubic, respectively. Furthermore, there are typical diffraction peaks of a Pt face-centered cubic, including Pt (111), Pt (200), Pt (220), and Pt (311) planes that clearly appeared at about 40 º, 46 º, 68 º and 81 º, respectively.

For all the heat-treated catalysts, their XRD patterns showed a shift of 2θ corresponding to Au phase to higher values, as described in Table 4.7. This result indicates the formation of an AuPt alloy. The Au (220) diffraction peak was selected for calculating the lattice parameters of all the heat-treated catalysts using Bragg's equation. The results are shown in Table 4.8.

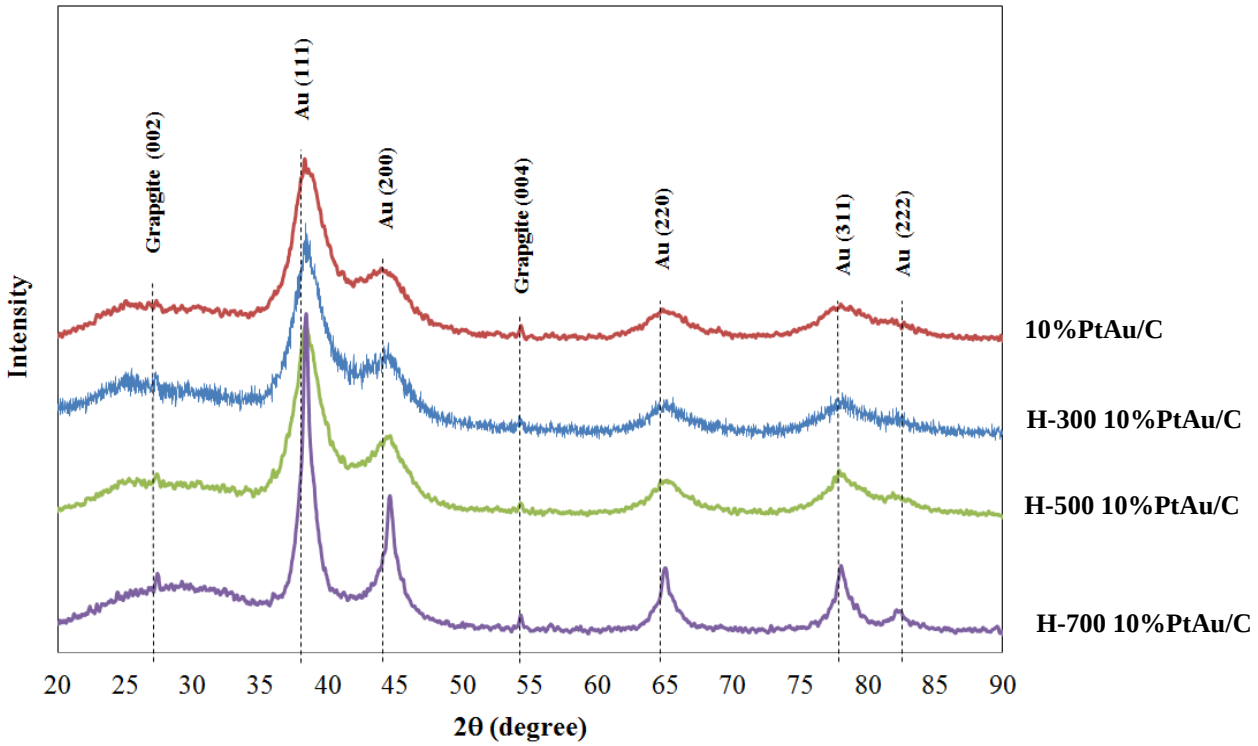

Figure 4.10 X-ray diffractograms of the untreated and heat-treated 10% PtAu/C catalysts.

The Au crystallite sizes of all the heat-treated catalysts were determined by Debye-Scherrer's Equation and the result are listed as shown in Table 4.8.

Table 4.8 Lattice parameters and crystallite sizes of untreated and heat-treated 10% PtAu/C catalysts.

Electrocatalyst	Crystallite size (nm)	Peak Position, θ_{max} (degree)	Lattice parameter (nm)
10% PtAu/C	2.7	65.14	0.4048
H-300 10% PtAu/C	2.8	65.15	0.4047
H-500 10% PtAu/C	3.1	65.20	0.4044
H-700 10% PtAu/C	5.9	65.24	0.4043

Furthermore, many researchers have claimed that heat treatment is an effective method to introduce more active catalyst sites by promoting alloy formation [11]. The lattice parameters from XRD results, as shown in Table 4.8, indicate that the higher heat-treatment temperature, the lower lattice parameter increasing the alloying degree

II. TEM characterization

The TEM images and of all heat-treated 10% PtAu/C catalysts are shown in Figure 4.11. The effect of heat treatment temperature on Pt particle sizes of the PtAu/C catalysts and their size distribution can be estimated. The size of particles was increasing with the increase of heat treatment temperature due to the sintering of the metal particles. As shown in Figure 4.11, it was clearly observed that the sintering of metal particles increased with the increase of temperature. The mean particle sizes of the metal particles calculated from the TEM images of all the heat-treated catalysts were in the range of 4.23-6.04 nm. The average diameters of H-300 10%PtAu/C, H-500 10%PtAu/C, and H-500 10%PtAu/C catalysts were 4.23 ± 0.8, 4.85 ± 0.92, and 6.04 ± 1.18 nm, respectively. These results of metal particle sizes were consistent with the XRD crystallite size.

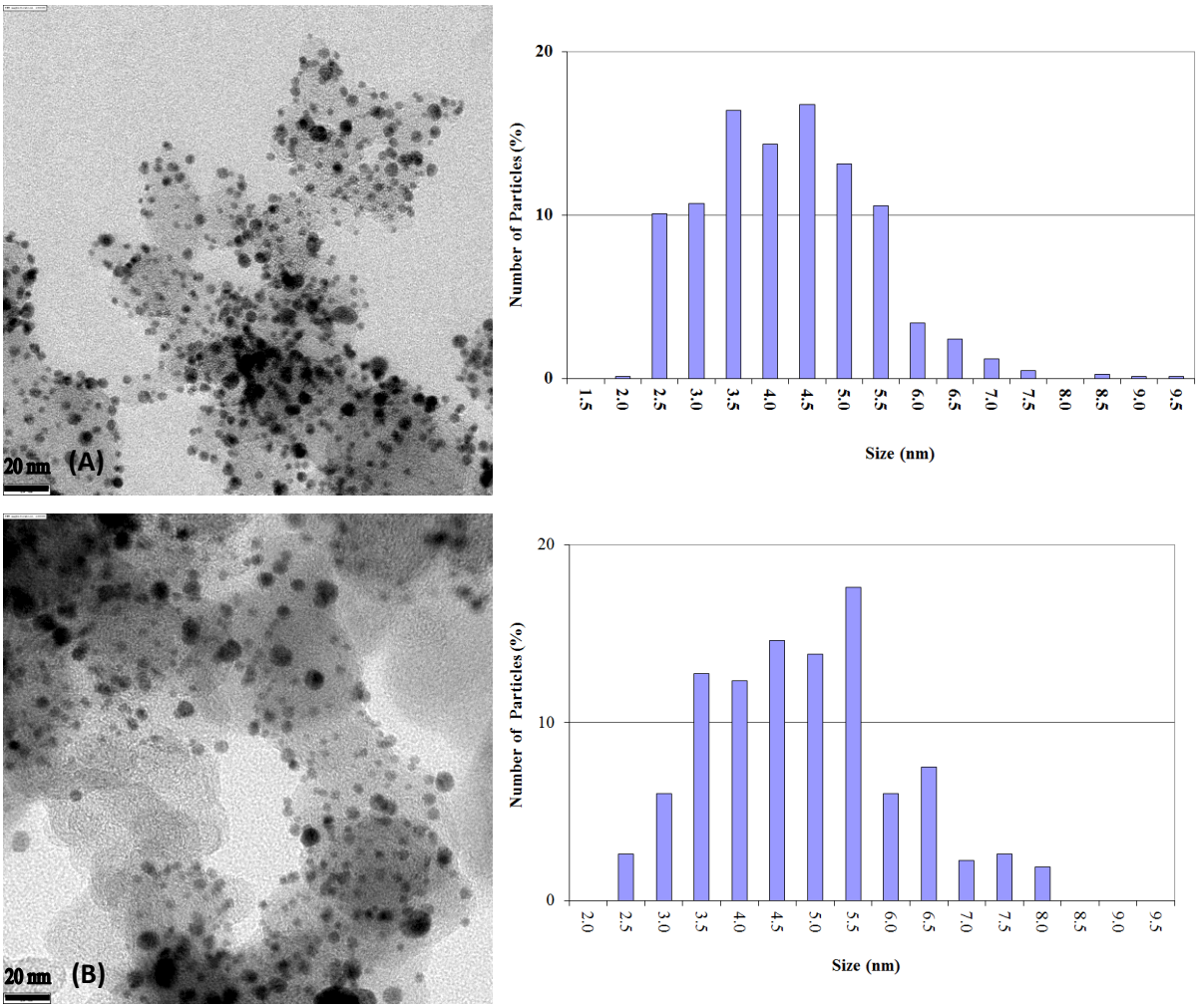

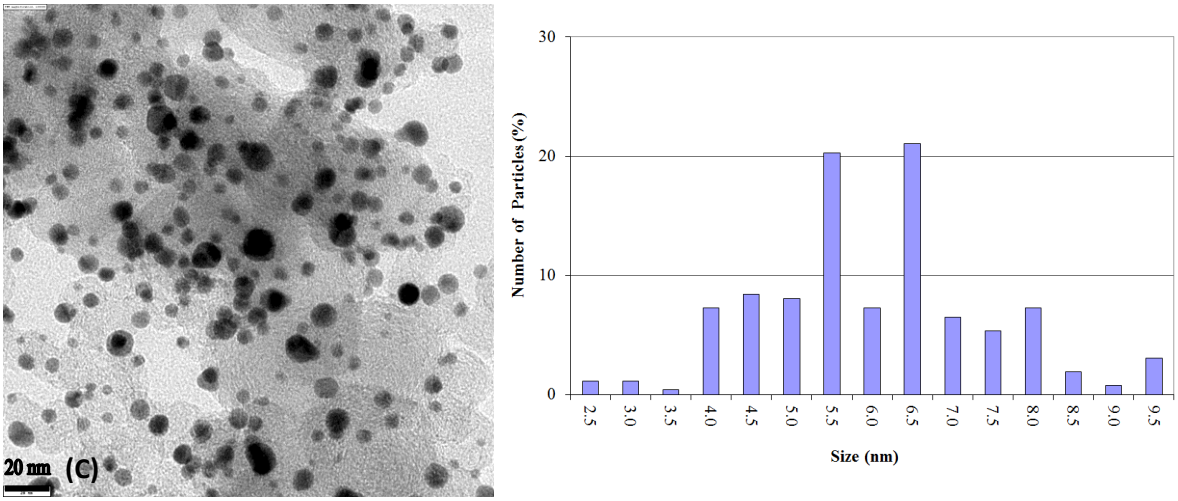

Figure 4.11 TEM images particle and size distribution of the heat-treated catalysts; (A) H-300 10% PtAu/C, (B) H-500 10% PtAu/C, and (C) H-700 10% PtAu/C.

Table 4.9 Particle sizes of untreated and the heat-treated 10% PtAu/C catalysts from TEM images.

Electrocatalyst	**Particle Size (nm)**
10% PtAu/C	3.81 ± 0.70
H-300 10% PtAu/C	4.23 ± 0.80
H-500 10% PtAu/C	4.85 ± 0.92
H-700 10% PtAu/C	6.04 ± 1.18

4.2.2 Electrochemical characterization of heat-treated 10% PtAu/C

Cyclic votammograms of the heat-treated catalysts in 0.1 M KOH are illustrated in Figure 4.12. In the positive scan, the oxidation of the gold surface occured at around 0.2 V., and in the negative scan, two reduction peaks of the reduction corresponding to the gold oxides appeared at approximately 0.05V. and -0.2V. refer to the reduction of quasi-2D and quasi-3D gold oxide states, respectively.

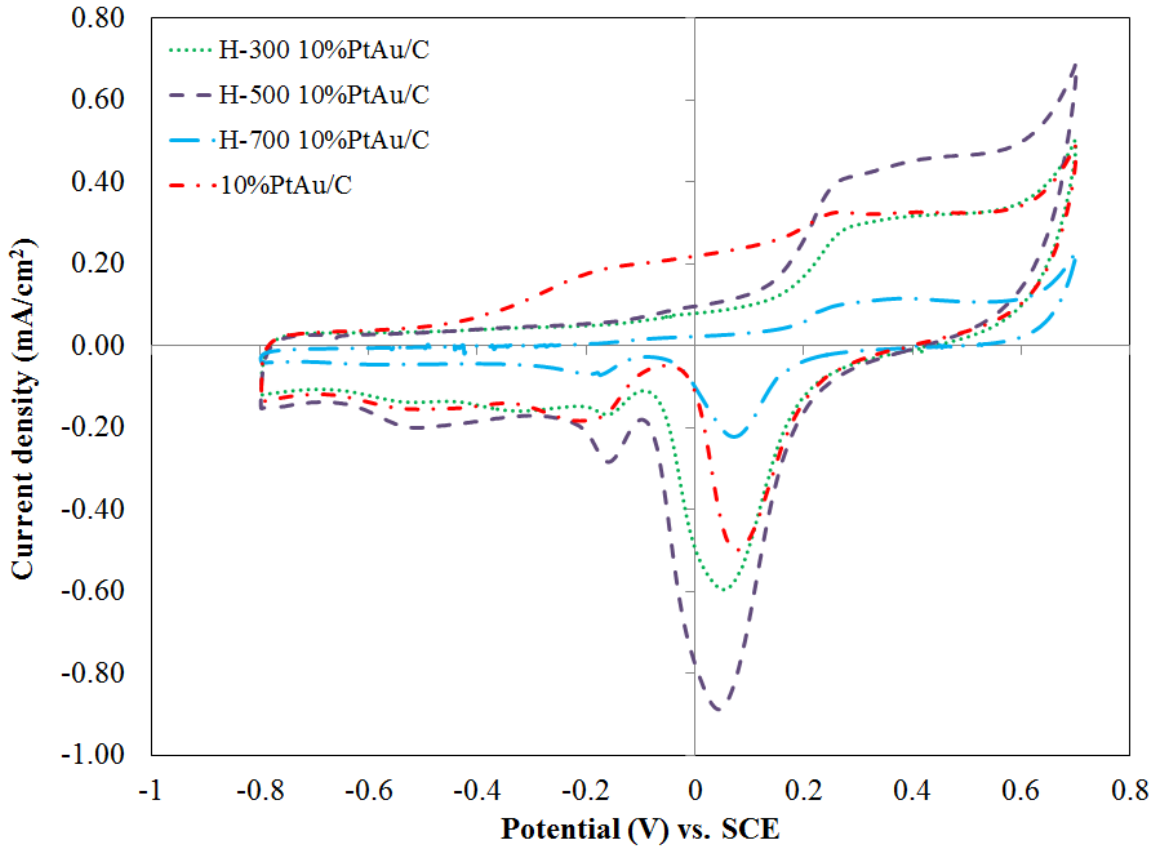

Figure 4.12 Cyclic voltammograms of the heat-treated catalysts in 0.1 M KOH solution with a scan rate of 0.02 $V.s^{-1}$ at 25ºC compared with that of untreated 10% PtAu/C.

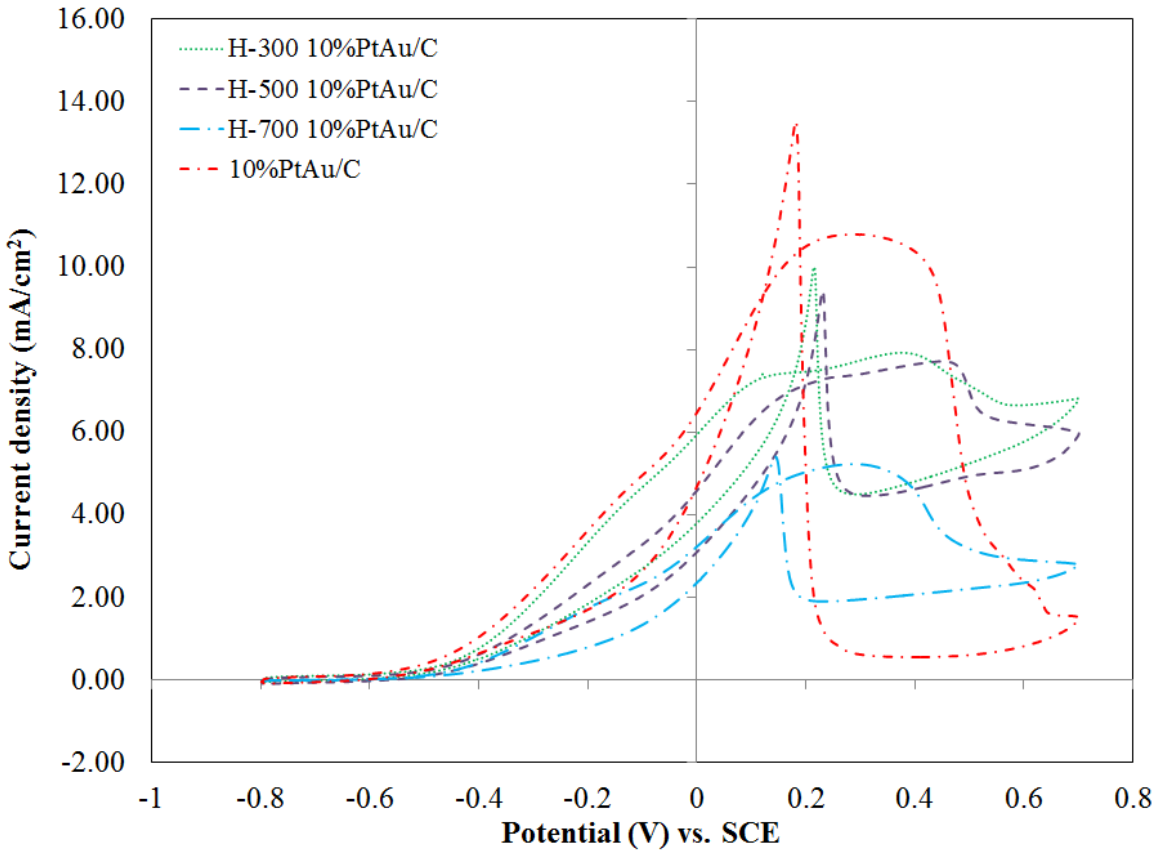

Figure 4.13 Cyclic voltammograms of the heat-treated catalysts in 0.1 M KOH solution containing 0.1 M glycerol with a scan rate of 0.02 $V.s^{-1}$ at 25ºC compared with that of untreated 10% PtAu/C.

Figure 4.13 shows the CVs of the as-prepared catalysts in 0.1M KOH containing 0.1M glycerol, the maximum current density obtained from H-300 10%PtAu/C, H-500 10%PtAu/C, and H-700 10%PtAu/C were 7.69, 7.78, and 5.22 mA cm^{-2} which are lower than the untreated PtAu/C. Among the heat-treated catalysts, the higher the heat treated temperature, the lower onset potential. Nevertheless, the catalyst yielding the lowest onset potential was still be the untreated PtAu/C. It was anticipated that the negative effect of the agglomeration of the catalysts particles in the heat-treated catalysts could overcome benefit obtained from the increase of alloying degree.

Table 4.10 Maximum current density and onset potential of heat-treated 10% PtAu/C catalysts.

Electrocatalyst	**Maximum current density ($mA.cm^{-2}$)**	**Onset potential (V vs. SCE)**
10% PtAu/C	10.79	-0.481
H-300 10% PtAu/C	7.69	-0.433
H-500 10% PtAu/C	7.78	-0.447
H-700 10% PtAu/C	5.22	-0.467

Chronoamperometric experiments were conducted to determine the stability of these catalysts by holding the potential at 300 mV vs. SCE for 60 min in 0.1 M KOH containing 0.1 M glycerol. The current produced from all catalysts drops rapidly during the first 2 min, and then decays slowly afterward (see Figure. 4.14). After holding the potential for 60 min, the final current density and decay rate of all catalysts were evaluated as concluded in Table 4.11. As heat-treatment temperature increased, the heat-treated PtAu/C gave a lower final current density and a higher decay rate. These results were caused by the agglomeration of the active metals as confirmed by the XRD and TEM results. Comparing the final current density, the catalyst stability of all the heat-treated and the untreated catalysts followed in descending order of 1

10%PtAu/C, H-300 10%PtAu/C, H-500 10%PtAu/C, and H-700 10%PtAu/C, which is consistent with the results of the particle size measured from the TEM images. At the same amount of active metal, the bigger particles provided less active surface area resulting in a lower final current density. Moreover, the chronoamperometric results were in good agreement with the cyclic voltammogram results. The agglomeration of particles caused the catalyst be less active and less stable.

The H-700 10%PtAu/C catalyst which has the lowest lattice parameter (or the highest alloying tendency) exhibited the lowest decay rate. This result suggested that AuPt alloy components in the catalyst enhance its stability toward glycerol electrooxidation.

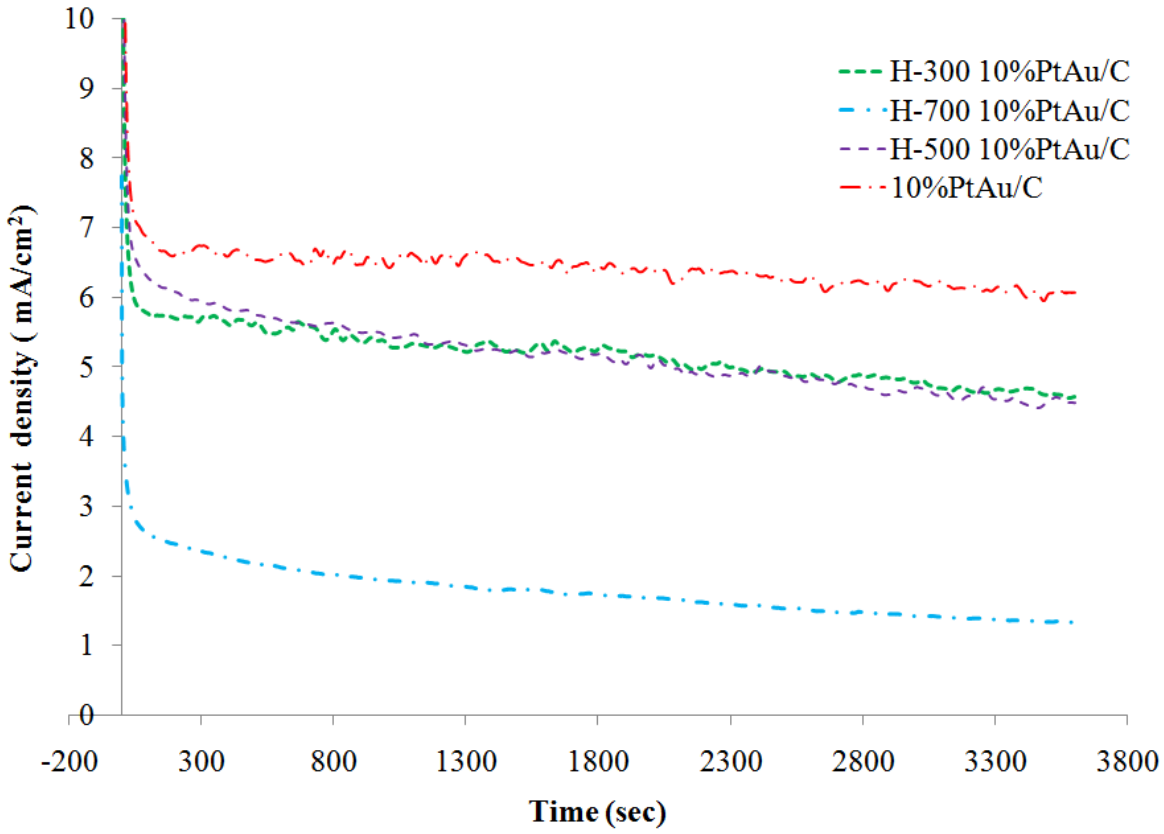

Figure 4.14 Chronoamperometric curves of the heat-treated catalysts catalysts in 0.1 M KOH solution containing 0.1 M glycerol compared with untreated 10% PtAu/C.

Table 4.11 Final current density and decay rate of untreated and heat-treated 10% PtAu/C catalysts.

Electrocatalyst	**Final current density ($mA.cm^{-2}$)**	**Decay rate ($10^{-3}\%.s^{-1}$)**
10% PtAu/C	6.066	2.827
H-300 10% PtAu/C	5.639	4.373
H-500 10% PtAu/C	7.148	4.486
H-700 10% PtAu/C	1.2953	1.327

CHAPTER 5
CONCLUSION

In this study, the Au-based catalysts were prepared by the PVA protection method. The metal precursors were mix before metal reduction and immobilization process. The surface morphologies of as-prepared catalysts were observed by using XRD and TEM. The crystal size of the catalyst was around 2.7-2.9 nm and the nanoparticles size was measured by using the image captured at magnification of 100,000. The average size of Pt/C was 2.34 nm and around 4 nm was noted as Au-based catalyst. Furthermore, The TEM images of Au/C and all bimetallic PtAu/C shown the well dispersion of metal on carbon supported. Contrastingly, the dispersion of Pt on Pt/C catalyst is not favorable caused by the strong interaction between PVA and the Pt atoms. The cyclic voltammogram and chronoamperometry were performed to investigate the catalytic behavior of the as-prepared catalyst. The CV result provides the 10% PtAu/C has higher current density and lower onset potential as compared to others. These might possibly occurs as the Pt in alkaline is active at low potential. The decaying rate of 10% PtAu/C is low which was examined from chronoamperometry.

The effect of heat treatment on the PtAu/C catalyst for glycerol electrooxidation in alkaline media was studied. Higher alloying degree of the heat-treated catalysts was achieved with the increase of heat-treated temperature. Consequently, the significant enhancement of onset potential of glycerol oxidation was taken place for the catalyst treated at 700°C. However, the heat treatment promoted sintering process of catalyst particle leading to the decreasing of the maximum current density. Therefore, the untreated PtAu/C showed higher performance than the heat-treated one.

REFERENCES

[1]. Bambagionia, V.; Bianchinia, C.; Marchionnia, A.; Filippi, J.; Vizzaa, F.; Teddyb, J.; Serpb, P.; Zhiania, M., (2009), Pd and Pt–Ru anode electrocatalysts supported on multi-walled carbon nanotubes and their use in passive and active direct alcohol fuel cells with an anion-exchange membrane (alcohol=methanol, ethanol, glycerol), *J. power sour.*, **190**, pp. 241–251.

[2]. Zhiani, M.; Gasteiger, H. A.; Piana, M.; Catanorchi, S., (2011), Comparative study between platinum supported on carbon and non-noble metal cathode catalyst in alkaline direct ethanol fuel cell (ADEFC), *Int. J. Hydrogen Energ*., **36**, pp. 5110-5116.

[3]. Falase, A.; Main, M.; Garcia, K.; Serov, A.; Lau, C.; Atanassov, P., (2012), Electrooxidation of ethylene glycol and glycerol by platinum-based binary and ternary nano-structured catalysts, *Electrochim Acta*, **66**, pp. 295– 301

[4]. Zhang, Z.; Xin, L.; Li, W., (2012), Electrocatalytic oxidation of glycerol on Pt/C in anion-exchange membrane fuel cell: Cogeneration of electricity and valuable chemicals, *Appl. Catal. B-Environ*., **119-120**, pp. 40-48.

[5]. Ishiyama, K.; Kosaka, F.; Shimada, I.; Oshima, Y.; Otomo, J., (2013), Glycerol electro-oxidation on a carbon-supported platinum catalyst at intermediate temperatures, *J. power sour.*, **225**, pp.141-149

[6]. Habibi, E.; Razmi, H., (2012), Glycerol electrooxidation on Pd, Pt and Au nanoparticles supported on carbon ceramic electrode in alkaline media, *Int. J. Hydrogen Energ*., **37**, pp.16800-16809.

[7]. Zhang, JH.; Liang, YJ.; Li, N.; Li, ZY.; Xua, CW.; Jiang, SP., (2012), A remarkable activity of glycerol electrooxidation on gold in alkaline medium, *Electrochim Acta*, **59**, pp. 156-159.

[8]. S. Yongprapat; A. Therdthianwong; S. Therdthianwong. (2012), Au/C catalyst prepared by polyvinyl alcohol protection method for direct alcohol alkaline exchange membrane fuel cell application, *J Appl electrochem*, **42**, pp. 483-490.

[9]. S. Yongprapat; A. Therdthianwong; S. Therdthianwong. (2012), RuO_2 promoted Au on C catalysts for alkaline direct alcohol fuel cells, *Electrochimica Acta*, **83**, pp. 87–93.

[10]. Yougui, C.; Lin, Z.; Juntao, L. (2007), Non-Pt anode catalysts for alkaline direct alcohol fuel cells, *Chin. J. Catal*., **28**, pp. 870-874.

[11]. Bezerra C. W. B.; Zhang, L.; Liu, H.; Lee, K.; Marques, A.L.B.; Marques, E.P.; Wang, H.; Zhang., (2007), A review of heat-treatment effects on activity and stability of PEM fuel cell catalysts for oxygen reduction reaction, *J. Power Sour.*, **173**, pp. 891–908

[12]. Jeon M.K.; Lee, K.R.; Jeon, H.J.; Woo, S.I., (2009), Effect of heat treatment on PtRu/C catalyst for methanol electro-oxidation, *J. Appl. Electrochem*., **39**, pp. 1503–1508.

[13]. Lamy, C., Lima, A., LeRhun, V., Delime, F., Coutanceau, C. and Lègar, J.M., 2002, Recent advances in the development of direct ethanol fuel cells (DAFC), *J. power sour.*, **105**, pp. 283-296.

[14]. Rousseau, S., Coutanceau, C., Lamy, C. and Lègar, J.M., 2006, Direct ethanol fuel cells (DAFC): electrical performances and reaction products distribution under operating conditions with different platinum-based anodes, *J. power sour.*, **108**, pp. 18-24.

[15]. Zhou, W., Zhou, Z., Song, S., Li, W, Sun, G., Tsiakaras, P. and Xin, Q., 2003, Pt based anode catalyst for direct ethanol fuel cells, *Applied Catalysis*, **46**, pp.273-285.

[16]. Antolini, E., 2009, "Carbon supports for low-temperature fuel cell catalysts, *Applied Catalysis*, **88**, pp.1-24.

[17]. Simões, F.C., dos Anjos, D.M., Vigier, F., Lègar, J.M., Hahn, F., Coutanceau, C., Gonzalez, E.R., Tremiliosi-Filho, G., de Andrade, A.R., Olivi, P. and Kokoh, K.B., 2007, Electroactivity of tin modified platinum electrodes for ethanol electrooxidation, *J. power sour.*, **167**, pp.1-10.

[18]. Fujiwara, N.; Siroma, Z.; Yamazaki, S.; Ioroi, T.; Senoh, H.; Yasuda, K. (2008), Direct ethanol fuel cells using an anion exchange membrane, *J. power sour*., **185**, pp. 621-626.

[19]. Varcoe, J.R.; Slade, R.C.T.; Yee, E.L.H.; Poynton, S.D.; Driscoll, D.J. (2007), Investigations into the ex situ methanol, ethanol and ethylene glycol permeabilities of alkaline polymer electrolyte membranes, *J. power sour*., **173**, pp. 194-199.

[20]. Yu, H. Y.; Krewer, U.; S. Keith, (2010), Principles and Materials Aspects of Direct Alkaline Alcohol Fuel Cells, *Energies*, **3**, pp.1499-1528.

[21]. Khan, A. S. A.; Ahmed, R.; Mirza, M.L., (2009), Evaluation of Catalytic Activity of Pt and Pt-Ru Catalysts or Electro-oxidation of Methanol in Acid Medium by Cyclic Voltammetry, *Port. Electrochim. Acta*, **27**, pp. 429-441.

[22]. Antolini, E.; Gonzalezb, E.R., (2010), Alkaline direct alcohol fuel cells, *J. power sour.*, **195**, pp. 3431–3450.

[23]. Matsuoka, K.; Iriyama, Y.; Abea, T.; Matsuoka, M.; Ogumi, Z., (2005), Alkaline direct alcohol fuel cells using an anion exchange membrane, *J. power sour.*, **150**, pp. 27–31.

[24]. Stuckey, P.A., (2012), *Kinetic studies and electrochemical processes at fuel cell electrodes*, Case Western Reserve University, USA.

[25]. Kwon, Y.; Lai, S.C.S.; Rodriguez, P.; Koper, M.T.M., (2011), Electrocatalytic oxidation of alcohols on Au in alkaline media base or gold catalysis, *J. Am. Chem. Soc*, **133**, pp. 6914–6917.

[26]. Jin, C.; Sun, C.; Dong, R.; Chen, Z., (2012), Electrocatalytic activity of PtAu/C catalysts for glycerol oxidation, *J. Nanosci. Nanotechnol*.,**12**, pp. 324–329.

[27]. Fang, Y. L., (2011), Understanding Structure-Property Relationships for Palladium-Gold Nanoparticles as Colloidal Catalysts, Houston, Texas, USA.

[28]. Jeon M.K.; Lee, K.R.; Jeon, H.J.; Woo, S.I., (2009), Effect of heat treatment on PtRu/C catalyst for methanol electro-oxidation, *J. Appl. Electrochem*., **39**, pp. 1503–1508.

[29]. Chen, W.; Tang, Y.; Bao, J.; Gao, Y.; Liu, C.; Xing, W.; Lu, T. (2007), Study of carbon-supported Au catalyst as the cathodic catalyst in a direct formic acid fuel cell prepared using a polyvinyl alcohol protection method, *J. Power Sour.*, **167**, pp. 315-318.

[30]. Hamelin, A. (1992), Surface crystallographic dependence of voltammetric oxidation of polyhydric alcohols and related systems at monocrystalline gold-acidic aqueous interface, *Langmuir*, **8,** pp. 975-981.

[31]. Baker, R.; Zhang, J., (2011), "Proton exchange membrane or polymer electrolyte membrane (pem) fuel cells". Available online: http://electrochem.cwru.edu/encycl /art-f04-fuel-cells-pem.htm

[32]. Gattrell, M., MacDougall, B. (2003). Reaction mechanisms of the O_2 reduction/evolution reaction In: Vielstich, W., Lamm, A. and Gasteiger, H.A. eds.,

Handbook of fuel cells fundamentals technology and applications. Volume 2: Electrocatalysis. West Sussex: John Wiley & Sons Ltd. pp.443-464.

[33]. "Direct Methanol Fuel Cell (DMFC)" Available online : http://www.machine-history.com/Direct%20Methanol%20Fuel%20Cell

[34]. Verykios, X. (2003), Support effects on catalytic performance of nanoparticles In: Wieckowski, A.; Savinova, E.R.; Vayenas, C.G. eds., Catalysis and electrocatalysis at nanoparticle surfaces. **Marcel Dekker**, Inc. America.

[35]. Watanabe, M. (2003), Design of electrocatalysts for fuel cells In: Wieckowski, A.; Savinova, E.R.; Vayenas, C.G. eds., Catalysis and electrocatalysis at nanoparticle surfaces. Marcel Dekker, Inc. America.

[36]. Kabbabi, A.; Faure, R.; Durand, R.; Beden, B.; Hahn, F.; Leger, J.M.; Lamy, C. (1998), In situ FTIRS study of the electrocatalytic oxidation of carbon monoxide and methanol at platinum-ruthenium bulk alloy electrodes, J. Electroanal. Chem., 444, pp. 41-53.

[37]. Amanda Quiroga (UCD) "Cyclic Voltammetry" Available online: http://chemwiki. ucdavis.edu/Analytical_Chemistry/Instrumental_Analysis/Cyclic_Voltammetry

[38]. "Introduction to Electrochemical Technique, Cyclic Voltammetry". Available online : http://220.227.100.58/Experiments/onlineExperiments/Experiment1/introduction.aspx

[39]. "Basic principle of Transmission Electron Microscope" Available online : http://www.hk-phy.org/atomic_world/tem/tem02_e.html

[40]. "Diagram outlining the internal components of a basic TEM system" (2009) Available online : http://commons.wikimedia.org/wiki/File:Scheme_TEM_en.svg

[41]. Wikipedia,"Powder diffraction", Available online: http://en.wikipedia.org/ wiki/Powder_diffraction

[42]. "Wide Angle X-ray Diffraction Studies of Liquid Crystals", Available online: http://cnx.org/contents/517f8f37-f619-4408-a8b4-2ef8a53e8c29@2

[43]. Sirlane G. da Silva; Júlio César M. Silva; Guilherme S. Buzzo; Rodrigo F.B. De Souza; Estevam V. Spinacé; Almir O. Neto; Mônica H.M.T. Assumpção. (2014), Electrochemical and fuel cell evaluation of PtAu/C electrocatalysts for ethanol

electro-oxidation in alkaline media, *Int. J. Hydrogen Energ*., **39** (19) pp. 10121–10127

[44]. Burke, L. and Nugent, P., (1997), Electrochemistry of Gold: I the Redox Behaviour of the Metal in Aqueous Media, *Gold Bulletin*, **30** (2), pp.43-53.

[45]. Li, M.F.; Liao, L.W.; Yuan, D.F.; Mei, D.; Yan-Xia Chen, (2013), pH effect on oxygen reduction reaction at Pt(111) electrode, *Electrochim. Acta*, **110** pp. 780–789

[46]. Mott, D; Luo, J; Njoki, P.N.; Lin, Y.; Wang, L.; Zhong, C.J., (2007), Synergistic activity of gold-platinum alloy nanoparticle catalysts, Catal. *Today*, **122, pp.** 378–385.

[47]. Gomes, J.F.; Tremiliosi-Filho, G., (2011), Spectroscopic Studies of the Glycerol Electro-Oxidation on Polycrystalline Au and Pt Surfaces in Acidic and Alkaline Media, *Electrocatal*, **2**, pp. 96–105.

[48]. Yu, E.H., Scott, S., Reeve, R.W. (2003), A study of the anodic oxidation of methanol on Pt in alkaline solutions, *J. Electroanal. Chem.* **547** pp.17-24.

[49]. Hernandez, J., Solla-Gullon, J., Herrero, E. (2004), Gold nanoparticles synthesized in a water-in-oil microemulsion: electrochemical characterization and effect of the surface structure on the oxygen reduction reaction, *J. Electroanal. Chem.* **574** pp. 185–196.

[50]. Padayachee, D., Golovko, V., Ingham, B., Marshall, A.T. (2014), Influence of particle size on the electrocatalytic oxidation of glycerolover carbon-supported gold nanoparticles, *Electrochim. Acta* **120** pp. 398–407.

APPENDIX A
CALCULATIONS

A.1 Catalyst preparation

A.1.1 Au/C Preparation : Prepare 100 mg of Au/C catalyst.

- Au Precursor

The amount of Au in final catalyst = 20 mg (20 wt% of metal loading)

20 mg (or 1.02×10^{-4} mol) of Au can be obtain from 40 mg of $HAuCl_4.3H_20$

Thus, 40 mg of $HAuCl_4.3H_20$ must be dissolved in 181.81 ml gain 110 mg l^{-1} of Au concentration in sol solution.

- PVA

The ratio of Au:PVA was 1:0.9 by mol. So, for 1.02×10^{-4} mol of Au, the certain amount of PVA was (1.02×10^{-4} mol x 0.9) x 44 g/mol_{PVA} x 1000mg/g = 4.04 mg

- $NaBH_4$

The ratio of Au:PVA was 1:4 by mol. So, for 1.02×10^{-4} mol of Au, the certain amount of $NaBH_4$ was 4.06×10^{-4} mol.

- Carbon

For 100 mg catalyst, weight of Au was 20 mg (20 wt% metal loading). Then, weight of carbon was (100-20) = 80 mg.

A.1.2 X%PtAu/C Preparation : Prepare 100 mg of X%PtAu/C catalyst. The percent of Pt in the bimetallic catalyst was 5%, 10% and 15%.

<u>5%PtAu/C catalyst</u>

- Metal Precursor

The average molecular weight of metal was (0.05x195.07 g/mol_{Pt}) + (0.95x196.97 mol_{Au}) = 196.87 g/mol_{metal}

The amount of metal in final catalyst was 20 mg (or 1.02×10^{-4} mol).

The amount of Au in final catalyst was 95%. Thus, the required amount of Au = 0.95 x (1.02×10^{-4}) = 9.65×10^{-5} mol_{Au} = 9.65×10^{-5} x 196.97 g/mol_{Au} = 19 mg_{Au}

19 mg of Au can be obtain from 38.02 mg of $HAuCl_4.3H_20$

The amount of Pt in final catalyst was 5%. Thus, the required amount of Pt = 0.05 x (1.02×10^{-4}) = 5.08×10^{-6} mol_{Pt} = 5.08×10^{-6} x 195.07 g/mol_{Au} = 0.99 mg_{Pt}

0.99 mg of Pt can be obtain from 2.63 mg of $H_2PtCl_6.6H_20$

Thus, 40 mg of metal precursor must be dissolved in 181.81 ml gain 110 mg l^{-1} of metal concentration in sol solution.

- PVA

The ratio of Metal:PVA was 1:0.9 by mol. So, for $1.02x10^{-4}$ mol of metal, the certain amount of PVA was ($1.02x10^{-4}$ mol x 0.9) x 44 g/mol_{PVA} x 1000mg/g = 4.04 mg

- $NaBH_4$

The ratio of Metal:PVA was 1:4 by mol. So, for $1.02x10^{-4}$ mol of metal, the certain amount of $NaBH_4$ was 4.06×10^{-4} mol.

- Carbon

For 100 mg catalyst, weight of metal was 20 mg (20 wt% metal loading). Then, weight of carbon was (100-20) = 80 mg.

The other platinum percent of bimetallic catalysts were calculated in this manner. The required amounts of the substances used in the preparation step are shown in Table A.1.

Table A.1 The amount of substances used in preparing 20 wt% of 10%PtAu/C and 15%PtAu/C.

	Au Precursor (mg)	**Pt Precursor (mg)**	**Dissolving in DI (ml)**	**$HAuCl_4$ (mol)**	**PVA (mg)**
10%PtAu/C	36.03	5.27	181.81	4.07×10^{-4}	4.02
15%PtAu/C	34.05	7.90	181.81	4.07×10^{-4}	4.03

A.2 Average Particle Sizes of Metal

The average size of Au nanoparticles was calculated from the measured value of at least 400 particles. The mean particle diameter (d_m) was calculated by using the formula:

$$d_m = \sum d_i n_i / \sum n_i \quad (A.1)$$

when n_i was the number of particles having the diameter d_i. The size deviating from the mean particle size is expressed by standard deviation, σ, which can be calculated by:

$$\sigma = [(d_i - d_m)P(x)]^{0.5} \quad (A.2)$$

when P(x) was a probability.

For example, the size of the black spots in the TEM image of AuL/C were measured and collected in Table A.2.

Table A.2 Raw data and the corresponding results from AuL/C TEM image.

Diameter (nm)	Counts	$d_i n_i$	P(x)
2.00	0	0	0.0000
2.50	36	90	0.0623
3.00	61	183	0.1055
3.50	164	574	0.2837
4.00	128	512	0.2215
4.50	118	531	0.2042
5.00	29	145	0.0502
5.50	28	154	0.0484
6.00	8	48	0.0138
6.50	2	13	0.0035
7.00	4	28	0.0069
Sum	578	2278	1.00

From the data in Table A.1, the value of d_m was equal to 2278/578 = 3.94 nm. The standard deviation was 0.6 nm. Hence, the average size of AuL/C was reported as 3.94 ± 0.6 nm.

A.4 d-spacing in electron diffraction pattern

The average crystallite size was estimated by the Debye-Scherrer formula :

$$d = \frac{0.9\lambda}{\beta \cos\theta} \qquad \text{(A.3)}$$

where d = the average crystallite size (nm)

λ = the wavelength of the X-rays (0.1540 nm)

β = the width of the peak at the half height (rad)

θ = the angle between the incident X-rays and the normal lattice plane (°)

The lattice parameter of Au can also be determined from Bragg's Law as follows:

$$n\lambda = 2d\sin\theta \quad \text{(A.4)}$$

And, the d-spacing formula for Face-centered cubic is shown in Equation (A.5) :

$$\frac{1}{d^2} = \frac{(h^2+k^2+l^2)}{a^2} \quad \text{(A.5)}$$

Then, we get

$$a = \frac{\sqrt{2}\lambda_{K\alpha_1}}{\sin\theta_{max}} \quad \text{(A.6)}$$

where a = lattice parameter of Au in Au (220) plane.

For example, Figure A.1 displays the Au (220) reflection peak of 10% PtAu/C, which is then fitted a Gaussian as shown by the red line.

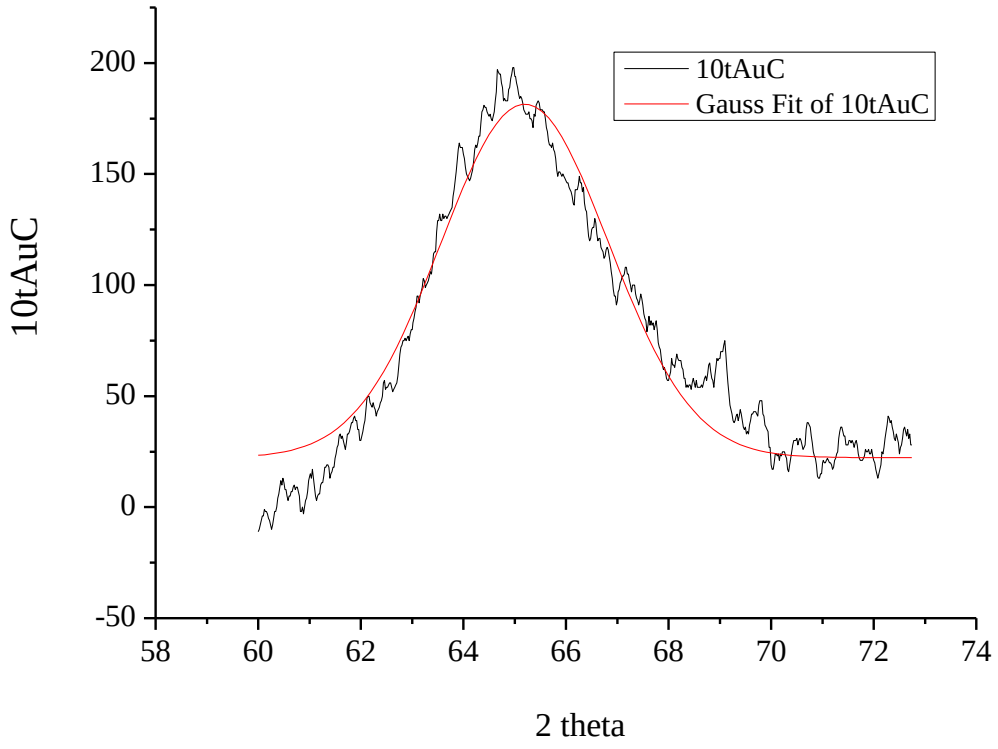

Figure A.1 The Au (220) reflection peak of 10% PtAu/C catalysts.

From fitting a Gaussian, the full width at half-maximum peak and angle at the maximum of the peak are 0.0673 rad and 32.59°, reapectively. Using Equations (A.3) and (A.6) to determine the crystallite size and lattice parameter.

So, K = 2.45 nm.

And a = 0.4045 nm.